AFRL-RX-WP-TR-2024-0045

ENGINEERING MICROORGANISMS TO INCORPORATE RARE-EARTH ELEMENTS INTO OPTICALLY ACTIVE INORGANIC NANOPARTICLES

Angela Belcher, Jifa Qi, Nimrod Heldman, Jay Sacane & Ngozi Eze
Massachusetts Institute of Technology, MIT

30 APRIL 2024
Final Report

AIR FORCE RESEARCH LABORATORY
MATERIALS AND MANUFACTURING DIRECTORATE
WRIGHT-PATTERSON AIR FORCE BASE, OH 45433-7750
AIR FORCE MATERIEL COMMAND
UNITED STATES AIR FORCE

NOTICE AND SIGNATURE PAGE

Using Government drawings, specifications, or other data included in this document for any purpose other than Government procurement does not in any way obligate the U.S. Government. The fact that the Government formulated or supplied the drawings, specifications, or other data does not license the holder or any other person or corporation; or convey any rights or permission to manufacture, use, or sell any patented invention that may relate to them.

Copies may obtain copies of this report from the Defense Technical Information Center (DTIC) (http://www.dtic.mil).

AFRL-RX-WP-TR-2024-0045 HAS BEEN REVIEWED AND IS APPROVED FOR PUBLICATION IN ACCORDANCE WITH ASSIGNED DISTRIBUTION STATEMENT.

DENNIS.PATRICK.BRIAN.1376889099 Digitally signed by DENNIS.PATRICK.BRIAN.1376889099 Date: 2024.07.02 15:06:29 -04'00'

PATRICK DENNIS
Project Engineer
Biomaterials Branch
Photonics, Electronics & Soft Materials Division
Materials and Manufacturing Directorate

MEADE.MITCHELL.LEE.1362279409 Digitally signed by MEADE.MITCHELL.LEE.1362279409 Date: 2024.07.02 15:11:47 -04'00'

MITCHELL MEADE
Deputy Branch Chief
Biomaterials Branch
Photonics, Electronics & Soft Materials Division Materials and Manufacturing Directorate

This report is published in the interest of scientific and technical information exchange, and its publication does not constitute the Government's approval or disapproval of its ideas or findings.

REPORT DOCUMENTATION PAGE

Form Approved
OMB No. 0704-0188

1. REPORT DATE *(DD-MM-YYYY)*	**2. REPORT TYPE**	**3. DATES COVERED** *(From - To)*
30 April 2024	FINAL	01 September 2022 – 30 March 2024

4. TITLE AND SUBTITLE
Engineering Microorganisms to Incorporate Rare-Earth Elements into Optically Active Inorganic Nanoparticles

5a. CONTRACT NUMBER
FA8650-22-2-7220

5b. GRANT NUMBER

5c. PROGRAM ELEMENT NUMBER
61101E

6. AUTHOR(S)
Angela Belcher, Jifa Qi, Nimrod Heldman, Jay Sacane & Ngozi Eze

5d. PROJECT NUMBER
DARPA

5e. TASK NUMBER

5f. WORK UNIT NUMBER
X22W

7. PERFORMING ORGANIZATION NAME(S) AND ADDRESS(ES)
Massachusetts Institute of Technology
77 Massachusetts Ave.
Cambridge MA 02139-43010

8. PERFORMING ORGANIZATION REPORT NUMBER
AFRL-RX-WP-TR-2024-0045

9. SPONSORING / MONITORING AGENCY NAME(S) AND ADDRESS(ES)
Air Force Research Laboratory
Materials and Manufacturing Directorate
Wright-Patterson Air Force Base OH 45433-7750
Air Force Materiel Command
United States Air Force

10. SPONSOR/MONITOR'S ACRONYM(S)
AFRL/RXEB

11. SPONSOR/MONITOR'S REPORT NUMBER(S)
AFRL-RX-WP-TR-2024-0045

12. DISTRIBUTION / AVAILABILITY STATEMENT
Distribution Statement A: Approved for public release: distribution is unlimited.

13. SUPPLEMENTARY NOTES
Report contains color.

14. ABSTRACT
REE doped materials are well known optical active materials widely used in display, LED, laser, phosphors applications. However, to the best of our knowledge, there has been no previous successful synthesis of sodium rare-earth fluoride NPs using biological route under mild aqueous conditions, as well as no report on successful aqueous synthesis of REE doped bio-lead halide perovskite materials. In this project, we have developed a novel bio-based two-step synthesis approach for high quality of bio- NaREEF4 nanoparticles. The synthesis involved aqueous synthesis of M13-phage templated bio-REE hydroxides as the precursors, and further fluoridation of bio-REE hydroxides in organic solvents to turn them to NaREEF4 nanoparticles. In a similar approach, the aqueous solution synthesized REE-doped bio-cesium lead hydroxide-REE (bio-CsPb-OH:REE) NPs as the precursors to synthesize halide perovskite (bio-CsPbX3:REE) NPs in organic solvents. Through this approach, we have demonstrated the ability to control the composition of the bio-REE NPs (e.g. Doped the one REE, two or more REEs with designed ratio), the particle size, uniformity and shape, PL efficiency, and material stoichiometry among the multiple elements in the NPs. The synthesis approaches developed in the project could provide alternate methods to produce very small, uniform high-emission, high-quantum yield biotemplated REE NPs (size <15 nm, QE >30%), and 1D and 2D nanomaterials under mild, aqueous conditions, which could be useful in many important applications such as biomedical near-infrared (NIR) imaging probes, photovoltaic devices, and phosphors for LEDs.

15. SUBJECT TERMS
Magnetically Active Rare Earth Element (REE), Biomineralization, Functionalized Protein, Advanced Characterization

16. SECURITY CLASSIFICATION OF:			**17. LIMITATION OF ABSTRACT**	**18. NUMBER OF PAGES**	**19a. NAME OF RESPONSIBLE PERSON**
a. REPORT	**b. ABSTRACT**	**c. THIS PAGE**			**19b. TELEPHONE NUMBER** *(include area code)*
Unclassified	Unclassified	Unclassified	SAR	43	Patrick Dennis (937) 255-9068

TABLE OF CONTENTS

LIST OF FIGURES

Figure **Page**

LIST OF TABLES

Table **Page**

1.0 SUMMARY

REE doped materials are well known optical active materials widely used in display, LED, laser, phosphors applications. However, to the best of our knowledge, there has been no previous successful synthesis of sodium rare-earth fluoride NPs using biological route under mild aqueous conditions, as well as no report on successful aqueous synthesis of REE doped bio-lead halide perovskite materials.

In this project, we have developed a novel bio-based two-step synthesis approach for high quality of bio- NaREEF4 nanoparticles. The synthesis involved aqueous synthesis of M13-phage templated bio-REE hydroxides as the precursors, and further fluoridation of bio-REE hydroxides in organic solvents to turn them to NaREEF4 nanoparticles. In a similar approach, the aqueous solution synthesized REE-doped bio-cesium lead hydroxide-REE (bio-CsPb-OH:REE) NPs as the precursors to synthesize halide perovskite (bio-CsPbX3:REE) NPs in organic solvents.

Through this approach, we have demonstrated the ability to control the composition of the bio-REE NPs (e.g. Doped the one REE, two or more REEs with designed ratio), the particle size, uniformity and shape, PL efficiency, and material stoichiometry among the multiple elements in the NPs.

The synthesis approaches developed in the project could provide alternate methods to produce very small, uniform high-emission, high-quantum yield biotemplated REE NPs (size <15 nm, QE >30%), and 1D and 2D nanomaterials under mild, aqueous conditions, which could be useful in many important applications such as biomedical near-infrared (NIR) imaging probes, photovoltaic devices, and phosphors for LEDs.

2.0 INTRODUCTION

Building on over 500 million years of evolution of natural biological systems, which have used biological templates for exquisite control over materials synthesis at the nanoscale, and building on extensive expertise in evolving biology for protein recognition and biotemplating of inorganic materials, the work below summarized the design and demonstration of biologically-enabled incorporation of rare earth elements (REEs) into inorganic nanoparticles (NPs), using various genetic and metabolic engineering approaches to fabricate REE-containing inorganic core-shell NPs (REE core-shell NPs). M13 bacteriophage (phage) is ideal for genetic engineering and nanomaterials design, as it 1) has a high-aspect-ratio filamentous structure; 2) has several types of modifiable exterior coat proteins; and 3) can be grown at scale and under a broad range of temperature and pH. The Belcher lab has extensive experience with fabricating biogenic and biosynthesized nanomaterials using M13 bacteriophage and yeast as chassis organisms.

We proposed to take a multi-pronged approach and simultaneously biosynthesize four classes of REE core-shell NPs using M13 bacteriophage as a genetically controlled biotemplate: (1) sodium rare-earth fluorides (core: $NaMF_4$, M = Y, Gd, or Lu, optionally doped with Yb and/or Er; shell: SiO_2, $NaYF_4$, CaF_2, or YF_3), (2) rare-earth doped oxides (core: Y_2O_3, ZnO; shell: Y_2O_3, Al_2O_3, SiO_2), (3) rare-earth perovskites (core: $LaYO_3$, $AlYO_3$, $SrTiO_3$, $CaTiO_3$, K_3InF_6:REE, Cs_3InX_6:REE [X = F, Cl], $CsMX_3$:REE [M = Yb, Pb; X = Cl, F; REE = Ce, Sm, Eu, Er, Tm, Yb]; shell: Y_2O_3, Al_2O_3, SiO_2, CaF_2, SrF_2, KF, $CsMX_3$), and (4) rare-earth organic-inorganic core-shell NPs (core: organic cryptate molecules complexed with Eu, Tb, or La ions; shell: inorganic – SiO_2, ZnO, SrO, TiO_2). Single-stranded DNA contained within the viral capsid encodes all proteins necessary for its assembly, and this DNA can easily be mutated in order to modify the exterior coat protein amino acid sequences or to display heterologous fusion proteins on the surface. This genotype-phenotype link allows for straightforward chemical tunability – DNA sequences can be engineered for protein assembly of phage into nanostructures, binding, capping, as well as for display of amino acid residues or peptide sequences that preferentially nucleate metal and semiconductor nanoparticles and/or chelate metal ions. Nearly 2700 copies of the same amino acid residues or peptide can be expressed along the length of the phage coat at the N-terminal end of the major coat protein pVIII, and other functionalities can be engineered into the capping proteins pIII, pVI, pVII, and pIX.

2.1 Sodium Rare-Earth Fluorides

To biologically synthesize sodium rare-earth fluoride core-shell NPs, we took two approaches: (1) nucleate REE core-shell NPs onto M13 bacteriophage coat proteins in a two-stage process, followed by post-synthetic annealing; and (2) synthesize small REE seed core NPs abiotically, adsorb the seed core NPs to M13 bacteriophage coat proteins and allow them to grow to the desired size. Once complete, we then grew an inert shell over the core NPs biologically and followed with an optional post-synthetic annealing step. To start, we focused on adapting the abiotic synthesis of α-phase $NaYbF_4$ core NPs doped with 2% Er, 2% Ce, and 10% Zn (MW = 260.49 g/mol) performed using a seed-mediated sequential growth strategy developed by the Belcher team (Figure 1).

2.2 Rare-Earth Doped Oxides

To biologically synthesize rare-earth doped oxide core-shell NPs, we used a two-stage process in which M13 phage-based REE oxide core NPs are first nucleated and then followed by synthesis of an inert shell, either biologically or abiotically.

Weak visible light absorption peaks have previously been observed for ZnO doped with Er, Pr, or Nd relative to undoped ZnO, attributed to transitions from the $^4I_{15/2}$ ground state to the $^2H_{11/2}$ and $^4F_{9/2}$ excited states in Er-doped ZnO; to f–f and $^1D_2$–$^3H_4$ transitions in Pr-doped ZnO; and to ($^4I_{9/2}$ → $^2K_{13/2}$ and $^4G_{7/2}$), ($^4I_{9/2}$ → $^2G_{7/2}$ and $^4G_{5/2}$), and ($^4I_{9/2}$ → $^4S_{3/2}$ and $^4F_{7/2}$) transitions in Nd-doped ZnO[3]. Here, we will use REE nitrates as a precursor (REE = Nd, Pr, Y, Gd, or La) and will initially spike in an REE dopant during phage-based biological synthesis of non-REE metal oxide core NPs (such as ZnO).

Rare-Earth Perovskites: Our strategies to synthesize biologically rare-earth perovskite NPs largely rely on modifications of a co-precipitation method that involves dissolving REE precursors in benign solvents in which engineered M13 phage are dispersed to promote spatially tunable nucleation of REE NP cores with a second step to promote the formation of inert shells. We synthesized REE-doped oxide perovskites using M13 phage as a biotemplate based on biological synthesis methods developed by the Belcher team for pristine M13 phage-templated strontium titanate and bismuth ferrite.

We adapted using abiotic methods, such as using oleylammonium bromide and zinc diethyldithiocarbamate ($Zn(DDTC)_2$) as stabilizing agents for $CsPbBr_3$ NP cores and ZnS shells, respectively, for compatibility with M13 phage and incorporation of REEs.

3.0 METHODS, ASSUMPTIONS, AND PROCEDURES

3.1 Sodium Rare-Earth Fluorides

Many natural mineral substances of fluorite exhibit fluorescence under ultraviolet light, a property that takes its name from fluorite. The fluorescence of fluorite may be due to rare earth impurities, such as REEs: yttrium and ytterbium, and natural fluorite containing such erbium impurities also displays up conversion fluorescence. Rare-earth doped nanometer sized particles of $NaREEF_4$ ($NaYF_4$:Yb,Er) have been extensively studied in recent years as up-conversion and down-conversion light emitting materials. Though many synthesis approaches for $NaREEF_4$ nanoparticles have been investigated, however, to the best of our knowledge, there has been no previous successful example of synthesis of sodium rare-earth fluoride core-shell NPs under mild aqueous conditions, as well as using the bio-synthesis approach, and all previous synthesis methods require high temperatures and organic solvents.

In this project, we have developed a novel bio-based two-step synthesis approach for high quality Bio-$NaREEF_4$ nanoparticles. The process involved aqueous synthesis of M13-phage templated bio-REE hydroxides as the precursors, and further fluoridation of bio-REE hydroxides in organic solvents to obtain $NaREEF_4$ nanoparticles.

3.1.1 Materials

The nitrate salts of erbium, yttrium and ytterbium, sodium hydrate, sodium trifluoroacetate, sodium oleate, 1-octadecene (ODE), oleic acid (OA), and oleylamine (OM) were purchased from Sigma-Aldrich. All chemicals were used as received. The trifluoroacetate salts of erbium, yttrium and ytterbium were bought from Rare Earth Products, Inc. and used as received.

The genetically engineered M13 bacteriophage were amplified using *Escherichia coli* bacterial medium and purified by standard PEG/NaCl precipitation method. Phage were further dialyzed against DI water (Millipore Milli-Q, 18.2 MΩ-cm) at room temperature over 24 hours to remove remaining ions. Following dialysis, the phage was re-dispersed in DI water at concentration of $4x10^{11}$/mL.

3.1.2 Synthesis Steps of Sodium Rare-Earth Fluorides

Figure 1 demonstrates the M13 phage-based bio-synthesis approach for Bio-NaREEF4 nanoparticles. For a typical synthesis of 1 mmol of bio-NaY0.78Yb0.2Er0.02F4 NPs, 250 mL of phage solution of concentration of 4E11/mL were prepared and vigorously stirred at room temperature over 1 hour. 20 ml aqueous solution containing 0.78mmol Y3+, 0.2mmol Yb^{3+} and 0.02mmol Er^{3+} was added to the phage solution and incubated over 1 hour at room temperature. Then 20mL of 0.25M NaOH solution were added into the solution. Soon after addition of NaOH solution, the clear phage-REE solution became foggy indicating the generation of REE-hydroxide nucleation/precipitation in the solution. To complete the reaction, the solution temperature was raised to 70 °C and kept at temperature for more than 12 hours. Then, NP

purification was carried out by filtration using 0.22μm or 0.45μm pore sized filters or by repeat centrifugations at 3000 rpm.

The dried product was re-dispersed into OA/OM/ODE solution, and the solution was heated at 90℃ for at least 12 hours followed by 1hr at 130℃ in vacuum to remove residual water. Then, the vacuum was stopped, and inert argon gas was flowed through the reactor (over the solution), while raising the temperature to 330℃ and maintaining the reaction at the temperature for the desired time (eg, 30min, 1h, 1.5h…). At the end of the reaction time, the heat is turned off, the sample is allowed to cool down, and the sample is washed with toluene/ethanol mixed solvents and collected through centrifugations.

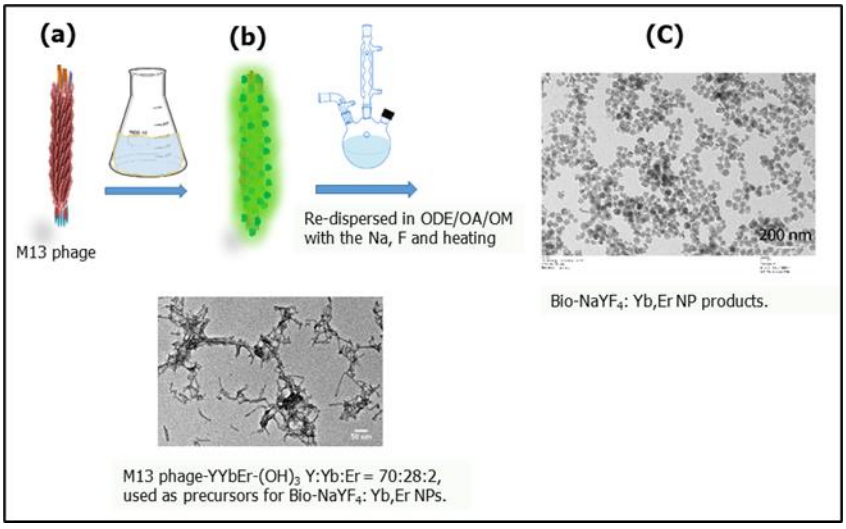

Figure 1. Scheme of M13-phage based bio-synthesis approach for bio-NaREEF4 NPs

Several control abiotic syntheses (without any biological molecule) experiments were carried out for comparison. The first was direct synthesis in the OA/OM/ODE mixed solvent solution, and using trifluoroacetate salts of sodium, erbium, yttrium and ytterbium as the precursors. All other procedures and conditions were the same as the biological synthesis counterparts. The second control abiotic synthesis is the same as the corresponding biological synthesis, using the two-step synthesis process and rare-earth nitrate salts (or chloride, acetate salts) as the precursors to get nanosized REE-hydroxides as the precursors which are then processed by following the synthesis process in OA/OM/ODE mixed solvent.

3.2 Rare-Earth Doped Oxides

Biologically synthesized rare-earth doped oxides are the basis for this research section. As we have reported in the earlier sections on bio-Na(REE)-fluoride NPs, forming bio-REE hydroxide nanomaterial is a crucial step, as it is used as a precursors for formation of bio-Na(REE)F_4. However, direct thermal treatment of the bio-REE hydroxide precursor will form bio-REE-oxide NPs. Moreover, bio-AB:REE$(OH)_x$ perovskite (where A, B are metals) could serve as a precursor for synthesizing bio-REE-doped perovskite oxide. We have synthesized bio-MO:REE (M = Zn, Sr, La, or Y; REE = Eu^{3+}, Tb^{3+}, or Nd^{3+}) (Figure 2) and bio-$SrAl_2O_4$:REE (REE=Eu^{2+}/Dy^{3+}; Eu^{2+}/Nd^{3+}) (Figure 2.2.2) in this research project. However, since these nanomaterials

required very high temperature treatment (700-1000°C), and their optical properties were not superior to the biosynthesized sodium yttrium fluoride-based materials, which were heated at much lower temperatures (~300-330°C), we eventually focused on the fluoride-based REE nanomaterials (section 3.1).

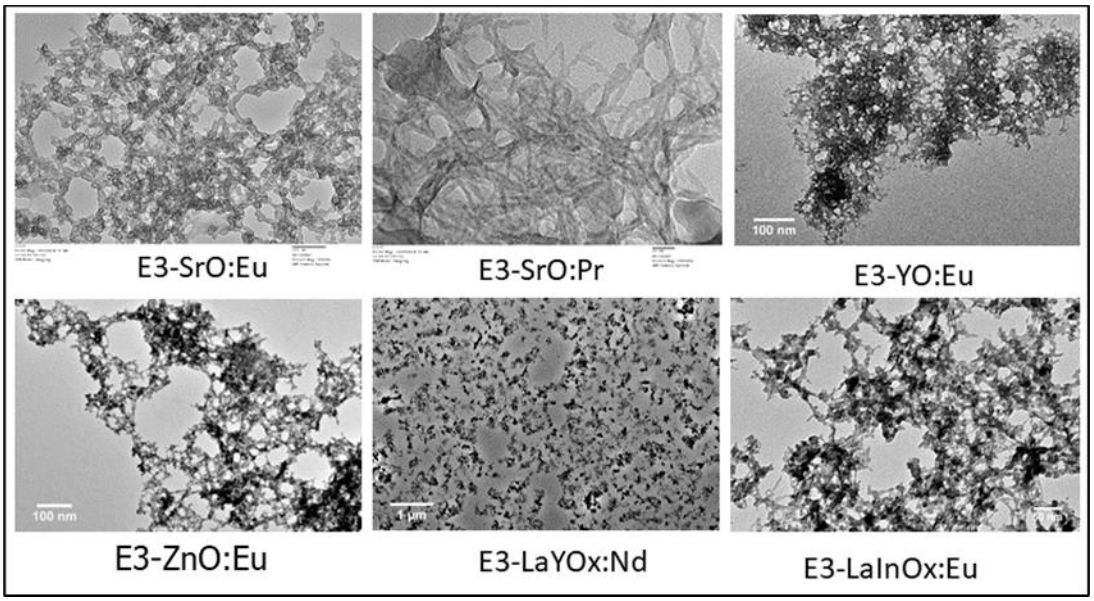

Figure 2. Bio-MO:REE NPs synthesized with E3-phage templates at mild temperature (from 21°C to 70°C).

3.2.1 Synthesis Steps of Rare-Earth Doped Oxides

Biologically synthesizing rare-earth doped oxides is very similar to the method presented for synthesizing the bio-REE hydroxide precursor in section 3.1. Mixing the host metal salt and doping agent REE salt with M13 phage in suspension, and then precipitating phage-metal complexes by increasing the pH to form phage-M:REE-(OH)x NPs. A purified powder of this product was treated at high temperature to form bio-MO:REE NPs.

3.3 Rare-Earth Perovskites

REE-doped oxide perovskites are an important type of opto/magnetic materials; however, they are very similar to the REE-doped oxides that required very high synthesis temperatures. Limited by the timescale of research project, we have not spent much effort redesigning the synthesis methods. However, we have still been able to biologically synthesize several bio-ABO_x precursors that are reported in Figure 2 [bio-$LaYO_x$:Nd, bio-$LaInO_x$:Eu, and the precursor bio-$YAlO_x$:Ce, Eu (YAP)].

Interestingly, the combination of lead halide perovskite and REE ions could combine the excellent optoelectronic properties of the host perovskite lattice with the f-f electronic transitions of the dopants, and such research could promote the further development of perovskites in the field of optoelectronics. We have started initial research on this topic.

3.3.1 Synthesis Steps of Rare-Earth Perovskites

Synthesizing rare-earth perovskites is similar to the synthesis of $Na(REE)F_4$; however there has been no successful aqueous synthesis of bio-lead halide perovskite reported to the best of our knowledge. To synthesize bio-lead halide perovskite NPs, our strategy is to adapt the aqueous solution synthesis of REE-doped bio-cesium lead hydroxide-REE (bio-CsPb-OH:REE) NPs as the precursors to synthesize halide perovskite (bio-$CsPbX_3$:REE) NPs in organic solvents. In a typical synthesis, EEAE-coated M13 phage was used as the biotemplate. To biologically synthesize rare-earth doped halide perovskite NPs, we combined ytterbium-doped cesium lead halide (Cl, Br) perovskite NPs ($CsPbCl_{3-x}Br_x$:Yb), 0.2 mmol lead acetate trihydrate [$Pb(OAc)_2 \bullet 3\ H_2O$], 280 µL of 1 M cesium acetate in ethanol, and 0.16 mmol ytterbium acetate hydrate [$Yb(OAc)_3 \bullet xH_2O$] in a 100 mL aqueous suspension of 5E13 total E3 phage particles and stirred at room temperature. After one hour, 1 mL 0.25 M NaOH solution was added to the suspension and stirred for 2 hours. Then, the bio-CsPbYb-OH precursor product was purified by repeat centrifugation at 3000 rpm and redispersion in H_2O/ethanol solution. The bio-CsPbYb-OH precursor was transferred to an organic solution of 10 mL octadecene, 1 mL oleylamine, and 2 mL oleic acid, and this solution was stirred and under vacuum at 70°C for 6 hours, then the temperature was raised to 110°C with degassing for 1 hour. Afterward, the flask was flushed with argon gas and heated to 240°C, followed by fast injection of 0.2 mL of chlorotrimethylsilane in 0.5 mL 1-octadecene. Immediately after injection, the flask was cooled to RT using a water bath, and the crude NP suspension was centrifuged at 3000 rpm for 15 min. The supernatant was discarded, and the pellet was suspended in hexane. The $CsPbX_3$:REE NPs were then washed once with ethyl acetate and centrifuged at 3000 rpm for 15 min. The supernatant was discarded, and the final pellet was resuspended in hexane.

4.0 RESULTS AND DISCUSSION

4.1 Physical Properties of Sodium Rare-Earth Fluorides

Figure 3 shows the typical biological synthesis of sodium rare-earth fluoride nanoparticles in this project. Figure 3a shows the M13 phage templated bio-YYbEr hydroxide product, which coated on the M13-phage (E3) formed wire like shapes. The initial stoichiometric ratio in REE nitrite salts was [Y]:[Yb]:[Er] = 78:20:2. The aqueous-solution synthesized products were purified and concentrated by a centrifugation/dispersion process. The products were lyophilized for use as the precursors of bio-$NaYF_4$:Yb, Er NPs. The dried powder was re-dispersed in a mixed organic solvent of octadecene, oleic acid and oleylamine., then Na, F precursor was added (sodium trifluoroacetate), and the solution was heated at higher temperature under Ar flow protection. Figure 3b and d demonstrated the bio-$NaYF_4$:Yb,Er NPs synthesized at 325°C in organic solvents. The data shows that the bio-YYbEr hydroxide precursor concentration in b is 9 times that in d; Figure 3c and e show the corresponding high magnitude zooming view and the FTT patterns of (b) and (d) respectively. The high precursor concentration resulted in better growth of the monocrystalline structure and a larger size particle (particle size in b: 70-80 nm and in d: 2-4 nm). In both synthesis conditions, bio-$NaYF_4$:Yb,Er NPs still maintained chain or wire like shapes suggesting that the templating effects of M13-phage still works well under these synthesis conditions. On the other hand, when we mixed E3 phages and trifluoroacetate salts of sodium, erbium, yttrium and ytterbium precursors in organic solvents of OA/OM/ODE, the synthesized NPs did not show any phage templating effects, no wire/chain like shape, and were not uniform in particle size or shape.

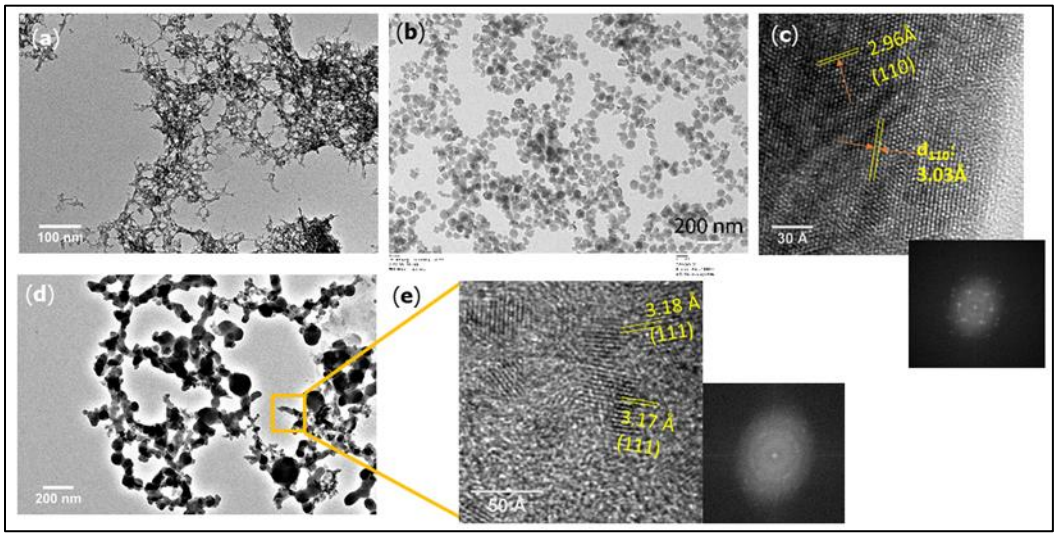

Figure 3. TEM images of biological synthesis of bio-NaREEF4 NPs: (a) Aqueous solution synthesis bio-REE hydroxide precursors; (b) and (d) The bio-NaYF4:Yb,Er NPs synthesized at 325°C in organic solvents. The precursor concentration in (b) is 9 times of that in (d); (c) and (e) The high magnitude zooming view and the corresponding FTT patterns of (b) and (d) respectively.

Thus, the aqueous synthesis of the bio-YYbEr hydroxide precursor is a key step for bio-$NaYF_4$:Yb,Er NP synthesis. To our knowledge, it was the first successful bio-aqueous synthesis approach for $NaREEF_4$ NPs.

To further evaluate the bio-templating effects and the stoichiometry of the bio-$NaYF_4$:Yb,Er NPs, we performed STEM-EDX (scanning transmission electron microscopy and energy-dispersive x-ray spectroscopy) experiments on the above bio-$NaYF_4$:Yb,Er NPs samples. Figure 4 shows the STEM image and EDX elemental mapping images of Na, Y, Yb, Er, F and P of sample #1 (low concentration) and sample #9 (high concentration). P are from the single stranded DNA of M13 phage which are distributed in wire-like network shapes, indicating that while the phage does not possess biological activity, the NPs still maintained the filamentous shape of the M13 phage. And around it, elements of Na, Y, Y, Yb, Er and F were distributed in the same shapes, either in the wire-like sample #1, or in the nanoparticle assembly sample #9. The data further confirmed that phage was effectively able to template in our synthesis approach.

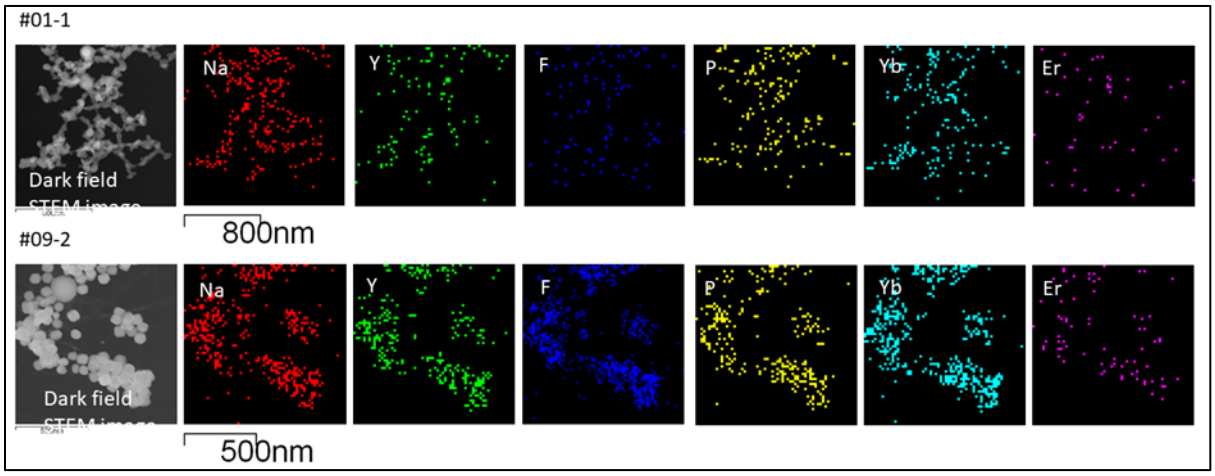

Figure 4. STEM-EDX elemental mapping of bio-NaYF4:Yb,Er samples showing all the elements of Na, Y, F, Yb, Er are overcoat on the bio-templates (P from DNA). Upper: corresponding to the lower precursor concentration sample #1 in Figure 2, lower, high concentration sample #9.

We further studied the crystal structures of bio-$REEF_4$ NPs compared with the control samples from abiotic synthesis. Figure 5 shows the XRD (X-ray diffraction) patterns of the bio-$NaYF_4$:Yb,Er NPs (sample #9) and the abiotic control obtained through the one-step organic approach. All abiotic control samples and #9 bio-$NaYF_4$ exhibit the same patterns corresponding to the β-$NaYF_4$ of hexagonal structures (pdf file: #00-064-0156). This also agrees with the HRTEM observations: the lattice fringes of hexagonal $NaYF_4$, with d110 ~ 2.96 – 3.03Å for sample #9 bio-$NaYF_4$:REE and the hexagonal FFT patterns. Because the quantity of lower precursor concentration were too low and had poor crystallinity due to the small size, we could not obtain high quality XRD results from the #1 and #9 bio-$NaYF_4$:REE NP samples. However, the HRTEM results suggest the structure corresponds to s cubic α-$NaYF_4$ structure, with a lattice distance of d111~0.317nm. Another important fact is that under the same heating temperature and duration, the aqueous-organic two-step abiotic synthesis yields a larger particle size at around 650 nm, while the one step organic abiotic synthesis yields a much smaller particle size

of 64.8 ± 6.1 nm, which is close to the sizes of two-step biologically synthesized particle #9 at about 66.2 ± 8.1 nm.

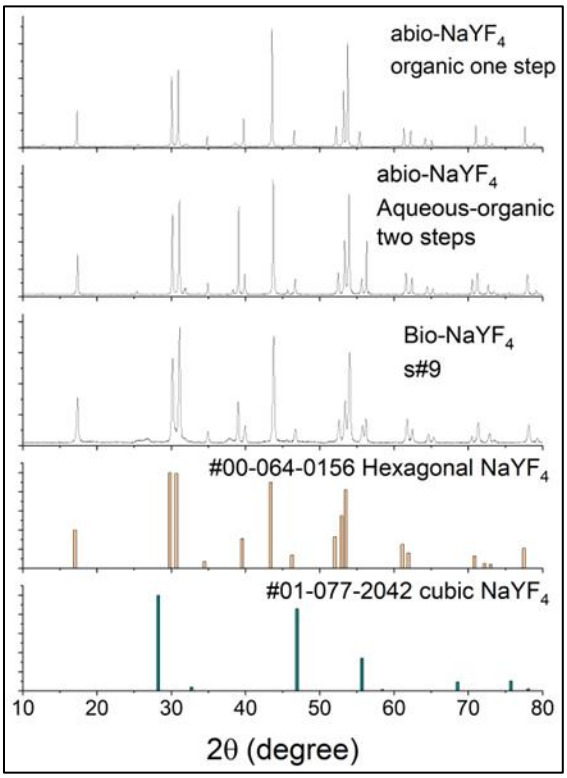

Figure 5. XRD (X-ray diffraction) patterns of the bio-NaYF4:Yb,Er NPs (sample #9) and the abiotic controls from different synthesis approach.

4.1.1 Functional Performance

The photoluminescence spectroscopy study of bio-$NaYF_4$:Yb,Er NPs (sample #1, 9) and the abio-$NaYF_4$:Yb,Er NPs were carried out for both up-conversion and down-conversion emissions (Figure 6) at room temperature under 980nm light excitations. The higher concentration precursors (#9 bio-$NaYF_4$:Yb,Er) resulted in better crystallinity, and therefore stronger and sharper emissions both in up-conversion (UC) and down-conversion (DC) photoluminescence (PL), while the lower concentration particles (#1 bio-$NaYF_4$:Yb,Er) led to continued smaller crystallites and weaker emissions. There is no significant difference in PL properties between the #9 bio-$NaYF_4$:Yb,Er and the control abio-$NaYF_4$:Yb,Er NPs. The attribution of REE optical transitions and the FWHM are shown in Figure 6.

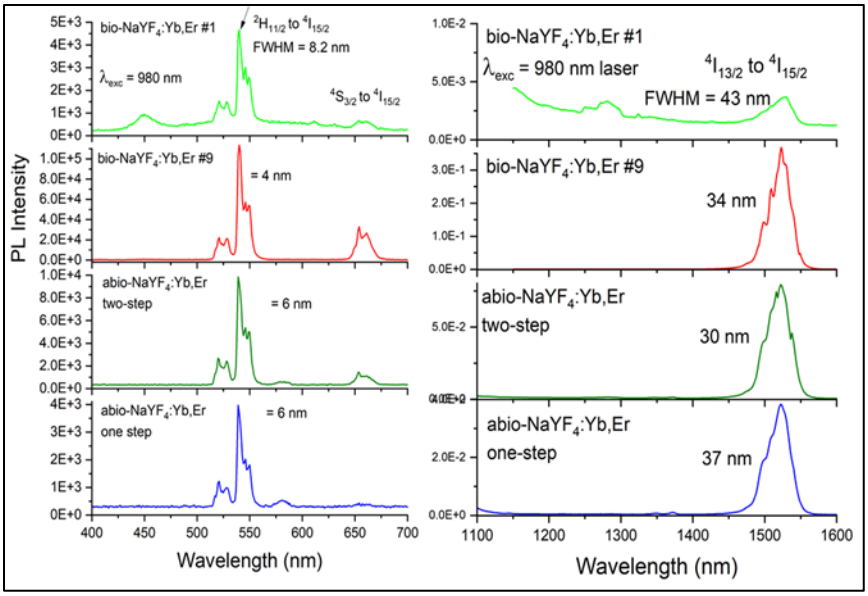

Figure 6. Room temperature PL spectra of bio-NaYF4:Yb,Er NPs (#1, #9) and abio-NaYF4:Yb,Er NPs synthesized at 325°C under the 980nm light excitations.

4.1.2 Tuning Properties and Performance

Like semiconductor quantum dots, core-shell structure REE NPs are an effective way to improve the light emission efficiency of REE. We investigated bio-REE core-shell nanostructures to improve the PL performance. Figure 7 shows bio-REE NPs and the correlated bio-REE core-shell NPs. The core bio-NaYbF$_4$:Er,Ce,Zn NP sizes are 10~20 nm, over which is a coating layer of NaYF$_4$:Yb with the thickness 5-6.5 nm forming the core-shell bio- NaYbF$_4$:Er,Ce,Zn@ NaYF$_4$:Yb NPs with sizes about 20~30 nm.

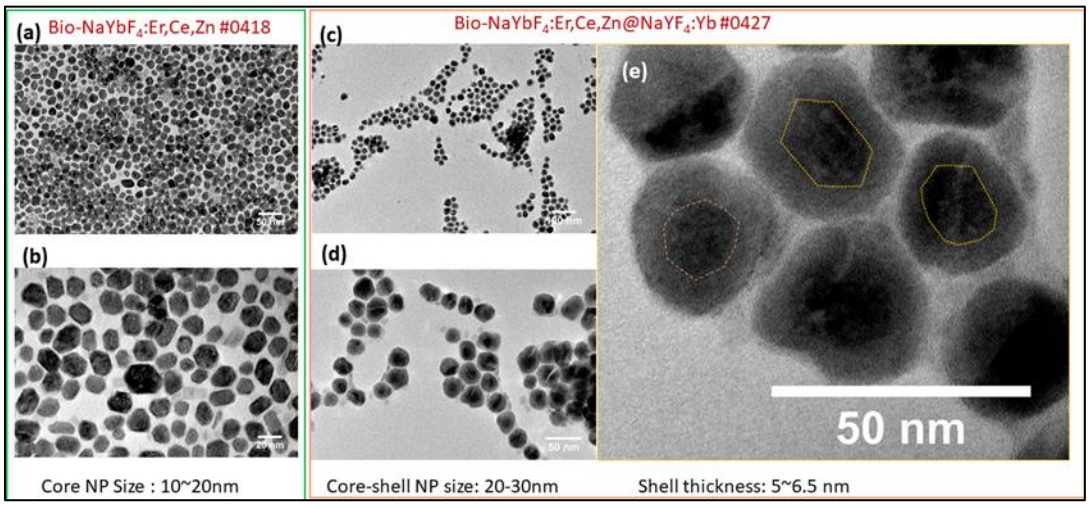

Figure 7. (a) and (b) TEM images of bio-NaYbF4:Er, Ce, Zn NPs at different magnitude; (c) to (e) TEM images of bio-NaYbF4:Er, Ce, Zn@NaYF4:Yb core-shell NPs at different magnitude.

Figure 8 shows the comparisons of PL from two types of bio-REE core and bio-REE core-shell NPs. Our data shows that the bio-REE core-shell structures enhanced PL intensity in both up-

conversion and down-conversion emission. The upper panel shows PL spectra from the pair of bio-$NaYbF_4$:Er, Ce, Zn core (red) and bio-$NaYbF_4$:Er, Ce, Zn@$NaYF_4$:Yb core-shell NPs (green). The enhancement factors are 13-fold for up-conversion and 1.6 fold for down-conversion emission. The lower panel compares the PL from the pair of bio-$NaYF_4$:Yb,Er core (black) and bio-$NaYF_4$:Yb,Er@$NaYF_4$:Yb core-shell NPs (red). The enhancement factors are 11.4 fold for up-conversion and 7.2 fold for down-conversion emissions. The PL enhancement of bio-REE-core-shell structures are attributed to the passivation of the surface defect states to decrease the non-radiative relaxation rates, and to the increase in light absorption in the cross section by the additional Yb^{3+} ions around the core-shell interfaces.

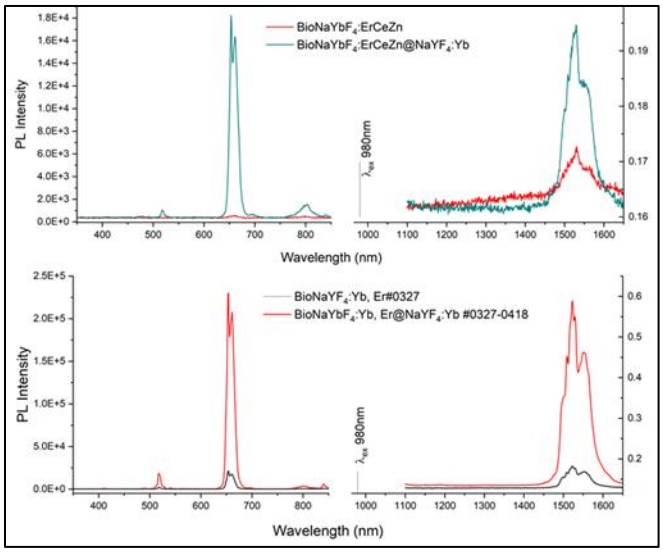

Figure 8. Comparison of PL from bio-REE core and bio-REE core-shell NPs. (Upper).bio-NaYbF4:Er, Ce, Zn core (red) and bio-NaYbF4:Er, Ce, Zn@NaYF4:Yb core-shell NPs (green); (bottom) bio-NaYF4:Yb,Er core (black) and bioNaYF4:Yb,Er@NaYF4:Yb core-shell NPs (red). Excitation 980nm light.

We further modified the synthesis of bio-$NaREEF_4$ NPs with a multi-hot injection technique. In this synthesis, we first re-dispersed bio-REE-hydroxide together with sodium oleate in a mixed organic solvent of octadecene, oleic acid and oleylamine., and heated the solution to 300℃, while stirring the solution with the Ar flow protection. We then injected Na, F precursors in the form of sodium trifluoroacetate in OA/ODE and kept heating the solution at 300℃ for 30 minutes and injection of Na, Y, Yb, Er, F precursors (trifluoroacetate salts in OA/ODE). We maintained heating at 300℃ for an hour for epitaxial growth of a layer of $NaYF_4$:Yb,Er over the bio-$NaYF_4$:Yb,Er NP core. After that, we further injected Na, Y, Yb, F precursors and maintained heating at 300℃ to grow shell layer $NaYF_4$:Yb over the NPs and forming the core-shell structure.

Figure 9 shows the examples of the multi-step injection approach to synthesis of bio-$NaYF_4$:Yb,Er@$NaYF_4$:Yb,Er (a-c) and bio-$NaYF_4$:Yb,Er@$NaYF_4$:Yb,Er@$NaYF_4$:Yb,Er (d-e).

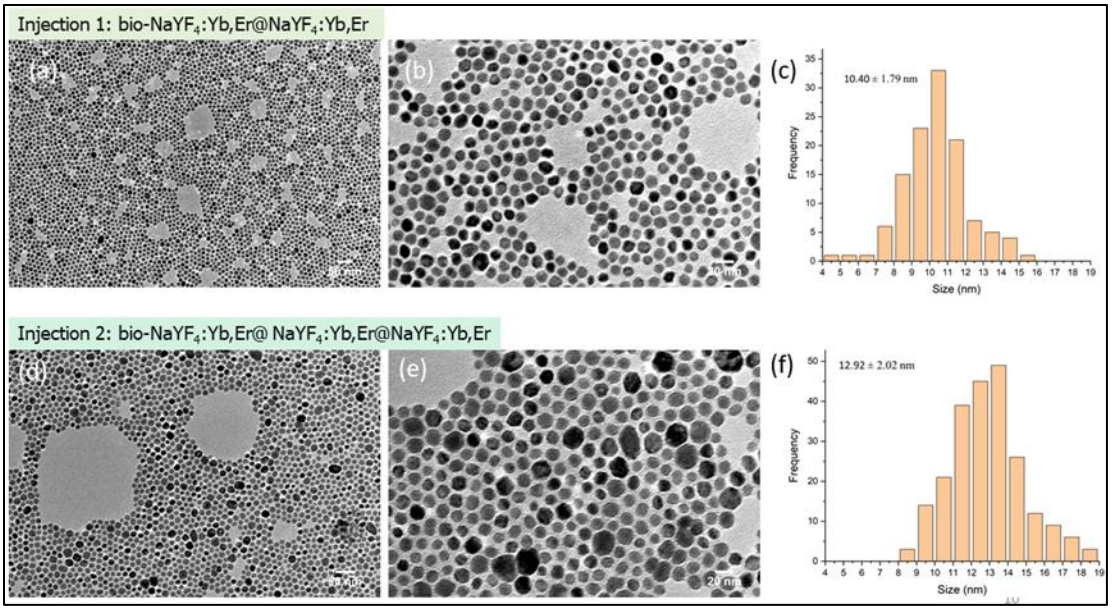

Figure 9. Multi-step injection approach to synthesis of bio-NaYF4:Yb,Er@NaYF4:Yb,Er (a-c) and bio-NaYF4:Yb,Er@ NaYF4:Yb,Er@NaYF4:Yb,Er (d-e).

This approach yielded uniform small size bio-REE NPs. In the example of the one-step injection sample bio-$NaYF_4$:Yb,Er@$NaYF_4$:Yb,Er, the size of the NPs is 10.40±1.79 nm, and in the case of the two-step injection sample, multilayered bio-$NaYF_4$:Yb,Er@$NaYF_4$:Yb,Er@$NaYF_4$:Yb,Er NPs displayed a NP size of 12.92±2.02nm. By tuning the amount of precursor in the injection, one can easily tune the thickness of the epitaxial layer and tune the size of the NPs. The advantage of this approach is both the tunability of particle size and the improvement of PL emission efficiency. Figure 10 shows the comparison of PL emission of NPs prepared through different approaches. It is notable that all bio-REE NPs perform better than that of abio-REE NPs, even in the case of very small particle size (11-12 nm). The multi-step injection (or multi-core-shell) sample demonstrated the highest down-conversion emission intensity, performing even better than the 40nm core-shell bio-REE NPs prepared by the previous method.

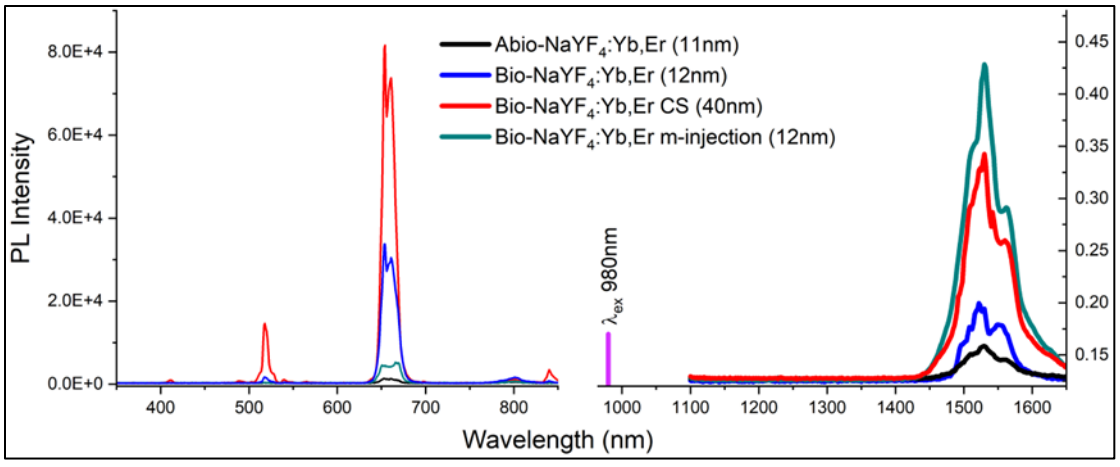

Figure 10. PL spectra of abio-NaREEF4 and abio-NaREEF4 NPs prepared through different approaches.

To more quantitatively describe the Pl emission of our bio-REE NPs, we have measured the PL efficiency and quantum yield of the samples. The PL efficiency is defined as the emitted power divided by the power absorbed by the material; and the quantum yield (QY), or the efficiency, is defined as the ratio of the number of the emitted photons to the number of the absorbed photons. The measurements were performed with a Thorlabs 4P3 Integrating Sphere setup. The setup included a highly stabilized 980 nm fiber coupled diode laser system as the excitation light source and optical filters (980nm notch filter and band pass filters) in front of the detector head (Thorlabs: S401C, 190-20,000nm) to avoid detection of the scattered laser and to measure the emission light of interest. The experimental results are listed in Table 1 for the down conversion emission. On our first attempt at measuring PL efficiency/quantum yield measurements, we focused on the down-conversion emission that peaked at 1540 nm, because the DC emission efficiency is higher than the UC. Abio-core-shell 0511 sample showed a 5.45% QY of Er^{3+} emission. However, bio-0706, even with no core-shell structure, showed better QY of 8.82%. Again, for the same molecular structure of sample, when adding a shell layer, biocs-0512-16-22 demonstrated a 18.8% QY. If we introduce additional doping with Ce and Zinc atoms then the UC process is quenched as we reported previously. Here we observed the further increase of QY up to 25.24%.

Table 1. Abio- and bio-REE NPs down-conversion PL efficiency and Quantum yield results

Sample	Comments	Efficiency, %	QY, %
Abio-cs-0511	abio-$NaYF_4$:Yb,Er@$NaYF_4$:Yb	3.5	5.45
bio-0706	bio-$NaYbF_4$:Er	5.67	8.82
bio-cs-0512-16-22	bio-$NaYbF_4$:Er@$NaYF_4$:Yb	12.08	18.8
bio-cs-sw0418	bio-$NaYbF_4$:Er,Zn,Ce@$NaYF_4$:Yb	16.22	25.24

4.1.3 Effect of Different Engineered Phage

In an aqueous solution of phage and REE ions, a fundamental process is the interaction of biomolecules with REE ions. For p8 type M13 phage, 2700 copies of surface coating proteins interact with REE ions. The interaction ability of different sequenced proteins and different REE ions could be different and could result in different final $NaREEF_4$ NP products, including the stoichiometry, shape, size and structures, and thus their physical properties. We have investigated the interactions of EEAE (E3), CPDC (Cys), DSPH, VSGSSPDS (P8#9) and AEGB (Wild-type) phage with ions of all 15 rare-earth elements (including Y, excluded Pm). We report on this in the following section. Here we will show results of bio-REE-hydroxide synthesized with five different phages. Figure 11 shows the TEM images of the synthesis of five different types of phage- REE-hydroxide NPs. All exhibited similar wire-like morphologies. Figure 11 also shows the TEM images of phage- $NaYF_4$:Yb,Er NPs synthesized with the above five different sequenced phages. The particle size, shape and uniformity of the samples made from different phage are quite different. EEAE and VSGSSPDS have the best control on uniformity of particle size. The average size of $NaYF_4$:Yb,Er NPs are 11.68±1.51(EEAE) and 58.81±9.23 nm (VSGSSPDS). The stoichiometry may also be different for the $NaYF_4$:Yb,Er particles made with different phages and it is important to have this information. Therefore, we analyzed the stoichiometric ratio through ICP-OES technique (Inductively coupled plasma optical emission spectroscopy). Figure 12d shows the ICP analysis results of the composition in molar ratio. The PL emission from samples made from different phages are also different as seen in Figure 12a-c.

ICP analysis results suggested the composition or the relative molar ratio of the REE elements are very close to the designed values and that could not be the dominating reason of the difference between these different $NaYF_4$:Yb,Er NPs. The main reason causing the difference of PL emission between these samples are due to the nano-crystalline size, crystalline qualities and particle size uniformities.

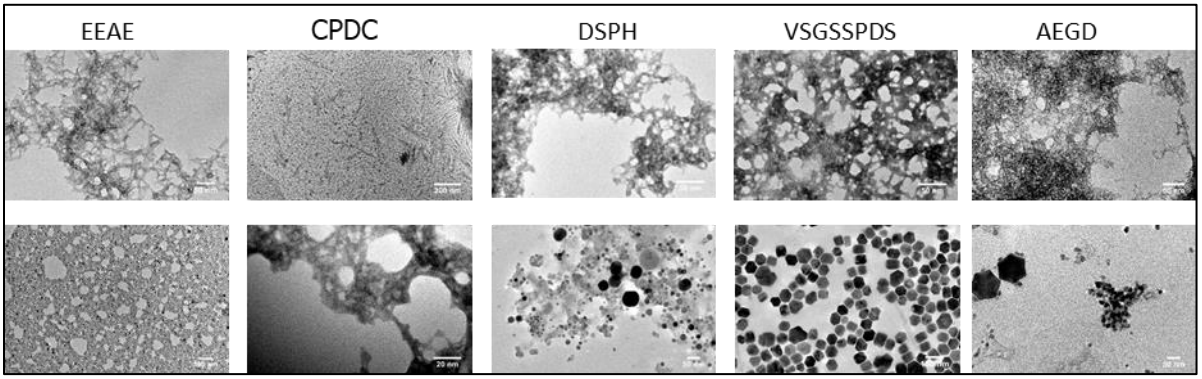

Figure 11. TEM images of phage-REE-hydroxide particles (up) and bio-NaYF4:Yb,Er NPs (bottom) synthesized with different sequenced engineered phages-at the same conditions.

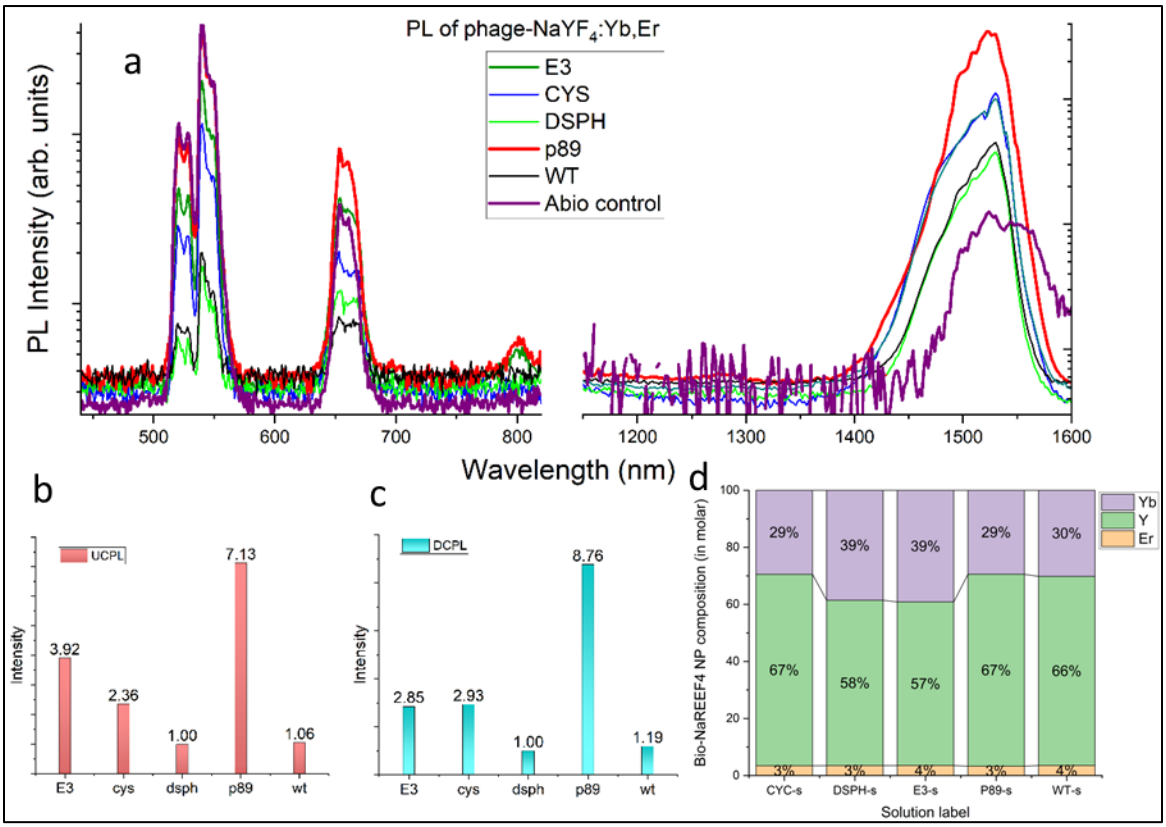

Figure 12. PL properties of the bio-NaYF4:Yb, Er NPs made from different type of phage; (a) UCPL and DCPL spectra; (b) UCPL (green emission band) and (c) DCPL peak intensity; (d) the molar ratio in each samples analyzed by ICP measurements.

4.1.4 Benchmark Abiotic

Abiotic approach synthesized abio-$NaYF_4$:Yb,Er, abio-$NaYF_4$:Yb,Er@$NaYF_4$:Yb core-shell NPs, abio-$NaYbF_4$:Er,Ce,Zn, abio-$NaYbF_4$:Er,Ce,Zn@$NaYF_4$:Yb, abio-$NaYF_4$:Yb, Tm were made for control comparisons and is reported in the previous section.

4.1.5 The Optical Transitions and the Fine Structure of the Emission Spectroscopy of bio-$NaYEEF_4$ NPs

As shown in the previous emission spectra (Figure 6, Figure 8, Figure 10, and Figure 12), the emission spectra of these bio-REE NPs consist of multi-emission peaks (or bands) and each transition peak consists of many fine structured spectral components. The whole emission spectral range covered a wide spectral regime from UV to NIR. The fine spectral structures in these bio-REE NP samples suggest that the good qualities of nanocrystalline structure such as the inhomogeneous broadening by lattice defects were not the dominating process for the emission spectral width. The effect was due to the inhomogeneous environments around the doping REE^{3+} centers that may slightly affect the REE^{3+} optical transition strength and energy level, resulting in the broadening spectrum and lower quantum yields. Further, we analyzed published literature which suggests a different attribution to the electronic transitions in these REE emission transitions and suggest that most of them might be typos or miss-citations. Thus, it is critical to carefully attribute each emission correlated electronic transition and the cause of the fine structures.

Figure 13 compared optical transitions in three bio-REE samples: 1) bio-REE NPs: $NaYF_4$:Yb,Er and 2) aa-$NaYF_4$:Yb,Tm NPs, with three REEs, two are optically active REEs; 3) bio-$NaYF_4$:Yb,Tm, Er, with four REEs, three are optically active REEs. The attributions of the emission peaks are labelled in the figure, which were compared with the theoretical and experimental results in the literature [1-6].

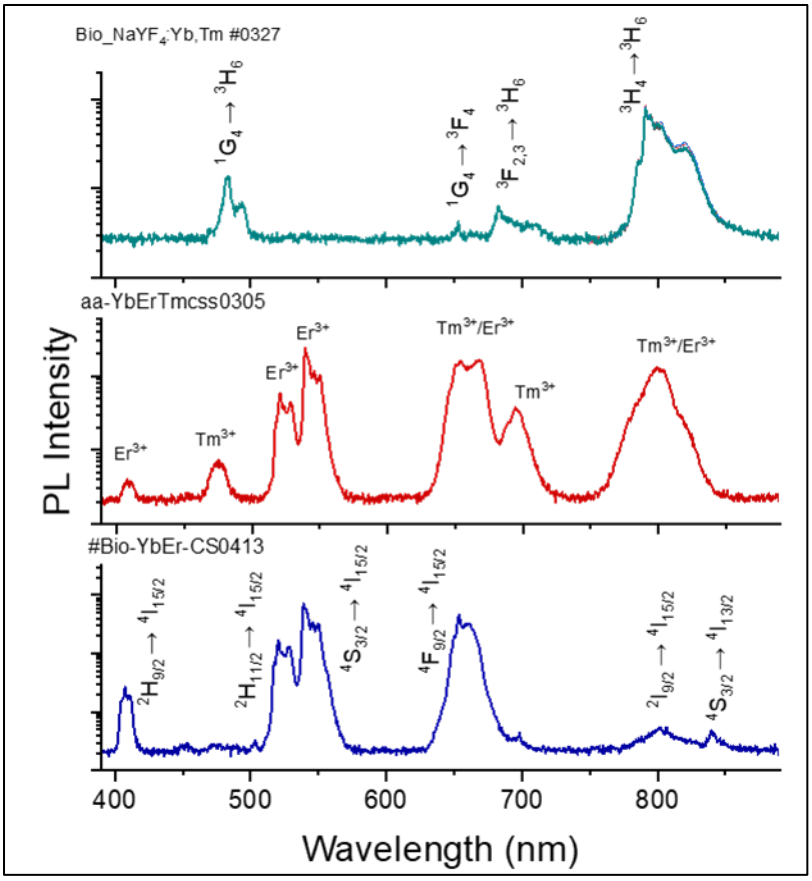

Figure 13. Up conversion emission spectra and the corresponding electronic transitions of bio-NaYF4:Yb,Er (bottom), bio-NaYF4:Yb,Tm (top) and NaYF4:Yb,Er, Tm (middle); the excitation light wavelength was 980nm.

Figure 14 compared up-conversion emission spectra of bio-$NaYF_4$:Yb,Er at room temperature and liquid nitrogen temperature (LN, 77K). The fine-spectral structures were observed both at room temperature and LN temperature. This is because all the observed spectral components were arising from the 4F inner shell electron transition, which was screen protected by the outer orbit electrons and less affected by environments in term of its energy level. The results of fitting the emission peak with multi-Gaussian functions were shown in Figure 14 b to e. For the transition of $^2H_{9/2} \rightarrow {}^4I_{15/2}$ (centered around 407nm), the average FWHM of the fine Gaussian spectral components are 2.6 nm and 2.1 nm at room temperature and liquid nitrogen temperature, respectively.

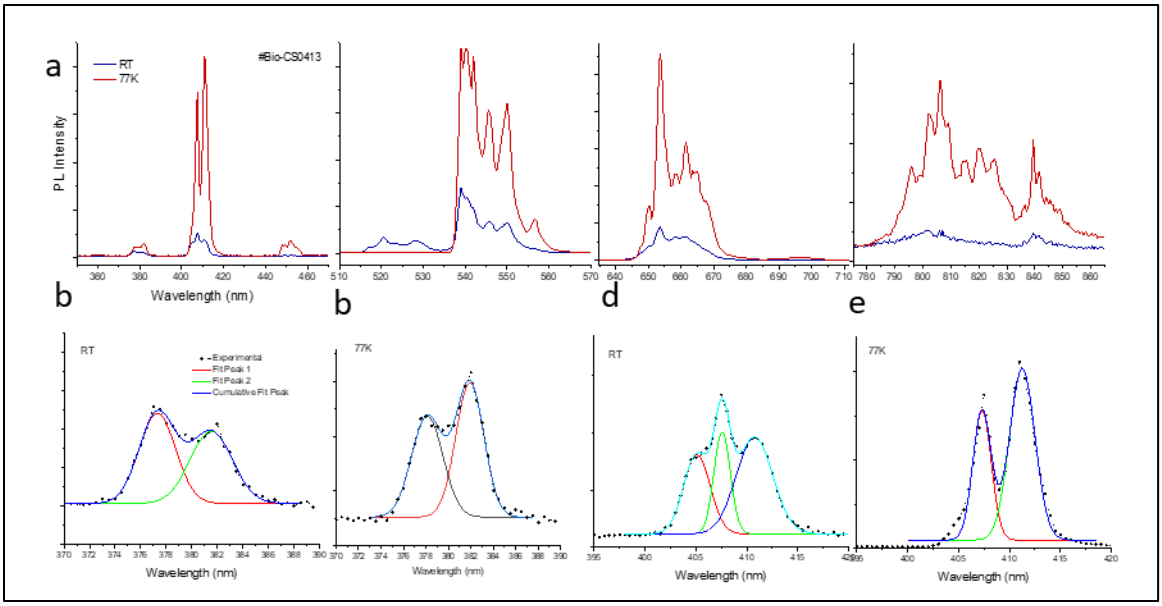

Figure 14. The up-conversion emission spectra of bio-NaYF4:Yb,Er at room temperature and liquid nitrogen temperature (a) and the multi-Gaussian function spectral fitting results for the emission peaks around 375 nm and 407 nm (b to e).

The down-conversion emission spectrum and the multi-Gaussian function fitting on the fine structures are shown in Figure 15. For the spectrum at LN temperature, it can be perfectly fitted with eight Gaussian peaks. The fitting results shows that the FWHM of the fine-structure peaks ranged from 1.57meV to 5.91 meV, with the average value of 3.38 meV, which is slightly less than reported 4.4meV [7] and much less than the Boltzmann energy k_B about 25.8 meV at room temperature and 6.62 meV at LN temperature.

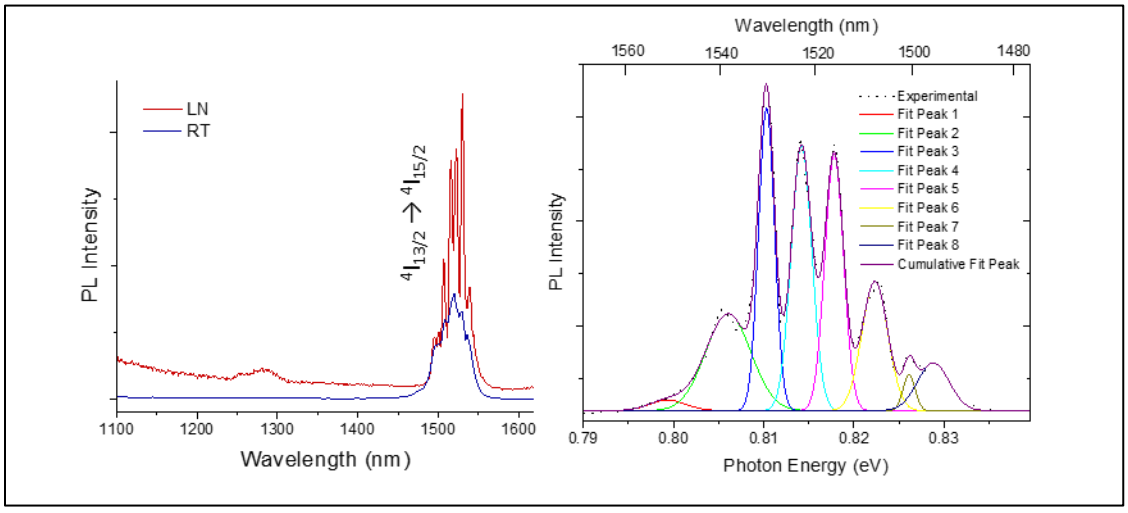

Figure 15. The down-conversion emission spectra of bio-NaYF4:Yb,Er NPs at room temperature and liquid nitrogen temperature (left) and the multi-Gaussian peaks fitting to the emission spectrum at liquid nitrogen temperature (right).

The fine-spectral structures of REE^{3+} are considered as the Stark's effect, the spectral line shifting and splitting causing the electric field. In the case of $^4I_{13/2} \rightarrow {}^4I_{15/2}$ transitions of Er^{3+},

both the energy levels of $^4I_{13/2}$ and $^4I_{15/2}$ are split into many closed sub-levels. Highly distinguished spectral fine-structures and the good fitting results enable us to compare with the theoretical results and the understanding of the local crystal field in bio-$NaYF_4$:Yb,Er NPs. [8]

4.1.6 Amino-Acid Mediated Synthesis of Sodium Yttrium Fluorides at Room Temperature

Inspired by the success in biological approach synthesis of REE doped sodium yttrium fluorides (e.g. $NaYF_4$:Yb, Er) though formation of REE hydroxides, we returned our interests back to the direct synthesis of sodium yttrium fluorides in an aqueous solution again.

We used REE salts (either nitrate, chloride, acetate) as the REE precursors, and the sodium fluoride (NaF) as the source of Na and F. We observed that the reaction of REE^{3+} with F^- and the nucleation of REE fluoride particles is a fast process whether in the presence of M13 phages or without phages. The synthesis produced larger sized homogenously precipitated particles of YF_3, YbF_3 sodium yttrium fluorides, and yttrium oxyfluorides in compositions as determined by XRD observations. Furthermore, particle sizes were beyond 200 nm with M13 phages and 400 nm without M13 phages. The results suggested that the peptides of phage do affect the reaction and nucleation process, however, the sorts of peptides and other reaction parameters need to be further modified to yield small size and single-phase sodium yttrium fluorides. The strategy of our approach allowed for decreasing the reaction speed by slowly injecting the reactants with a springe pump and using amino acid molecules to mediate the reactions instead of polypeptides from the bacteriophages. The resulting products were characterized by the TEM, XRD and PL spectroscopy.

TEM images shown in Figure 16 demonstrated that the improved synthesis approach yielded highly pure single phased nanoparticles in crystalline or amorphous structure. The different morphologies of the particles also suggested the different interaction mechanisms between amino acid molecules and sodium yttrium fluoride and their precursors. Similarly, XRD measurement results also show the purity of the products (Figure 17). All products are considered single phased sodium yttrium fluoride. The abio-sample showed a cubic structure, and amino acid assisted samples showed a hexagonal structure (eg. HIS and ILE) or amorphous structure (LYS). The sample synthesized with sodium glutamate mediation showed the amorphous and nanocrystalline in cubic structures. Table 4 lists the room temperature amino acid mediated synthesized sodium yttrium fluoride nanoparticle shapes, structures and product yield.

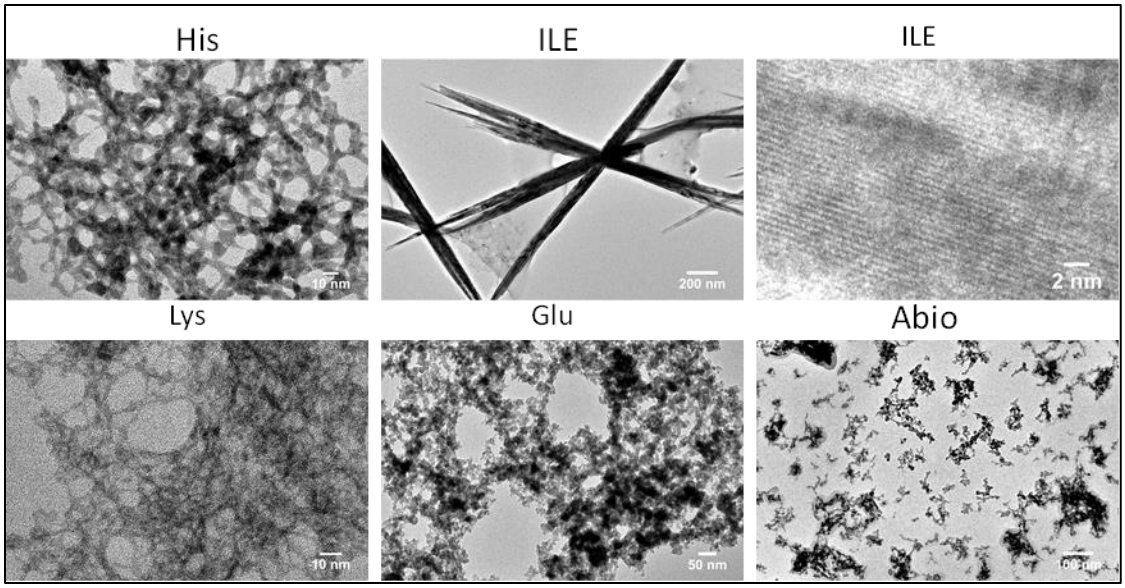

Figure 16. Typical amino acid mediated synthesized sodium yttrium fluoride nanoparticles and abiotic synthesized control. The lattice fringes view HRTEM image also showed.

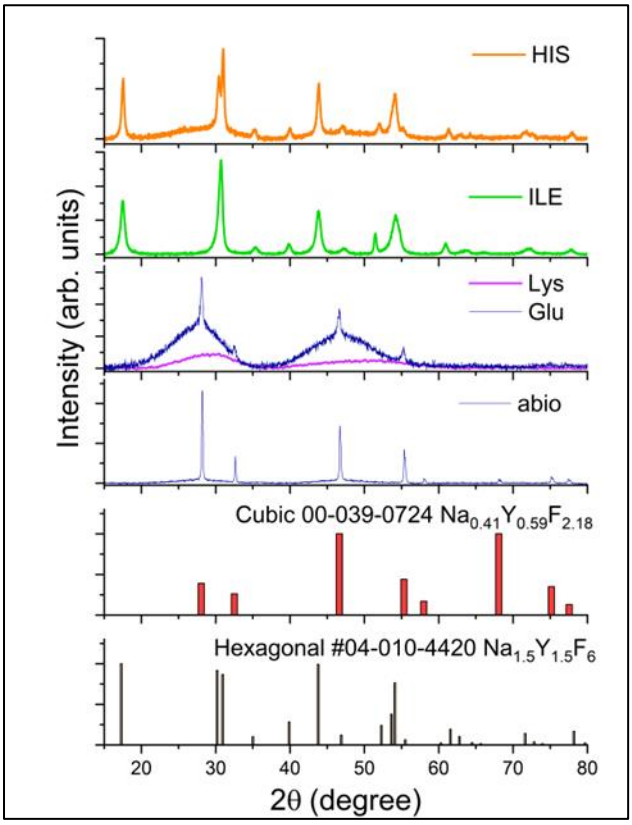

Figure 17. XRD patterns of amino acid mediated synthesized sodium yttrium fluoride particles and abiotic control sample. The standard JCPDS patterns were presented for comparison.

The tuning ability in crystalline structure and morphologies by amino acid molecules provided us a scope to understanding the biomolecules and microorganism interactions with the heavy metal ions, and a way to design novel materials in specific shapes and structures. Furthermore, amino-

acid mediated synthesis of REE NPs can be easily scaled-up at very low cost. Figure 18 demonstrates a synthesis of amino acid (glycine) mediated synthesis of sodium yttrium fluoride with a dried powder yield of 5.0 grams, consisting of 2.4 grams of REE.

Figure 18. 2 liter aqueous solution amino acid (glycine) mediated synthesis of sodium yttrium fluoride yield 5 grams product, which contains about 2.4 gram REE elements.

Dry powders of room temperature amino acid mediated synthesized particles can be directly annealed at higher temperatures turning into the optically active materials or suspended in the mixture solvent of OA/OM/ODE and following the same procedures heating at high temperature (eg. 300℃) to form sodium yttrium fluoride NPs and even the core-shell structure NPs as the photoluminescent nanomaterials. Figure 19 shows the TEM images of directly synthesized ytterbium and erbium doped sodium yttrium fluoride NPs with amino acid tyrosine mediation at room temperature, 90℃, and annealed at 240 and 300℃, respectively. Room temperature products are highly amorphous nanowire-like materials, while annealing at 300℃ resulted in aggregations of small nanocrystals of sodium yttrium fluorides. Figure 20 further compared NPs with abiotic samples that were directly synthesized at room temperature and annealed at 300℃. The annealing treatment at 300℃ of valine mediated synthesized particles converted the materials into 0.5 μm sized cubic particles. The 300℃ annealed abio-synthesized particles are much larger around 2 μm in hexagonal disk shapes. It is promising that the samples annealed in OA/ODE/OM mixed solution yield small sized uniform particles, suggesting room temperature amino-acid mediated directly synthesized sodium yttrium fluoride could be an alternate precursor for synthesis of sodium yttrium fluoride based up-conversion and down-conversion light emitting nanomaterials, with low cost and easy scale-up.

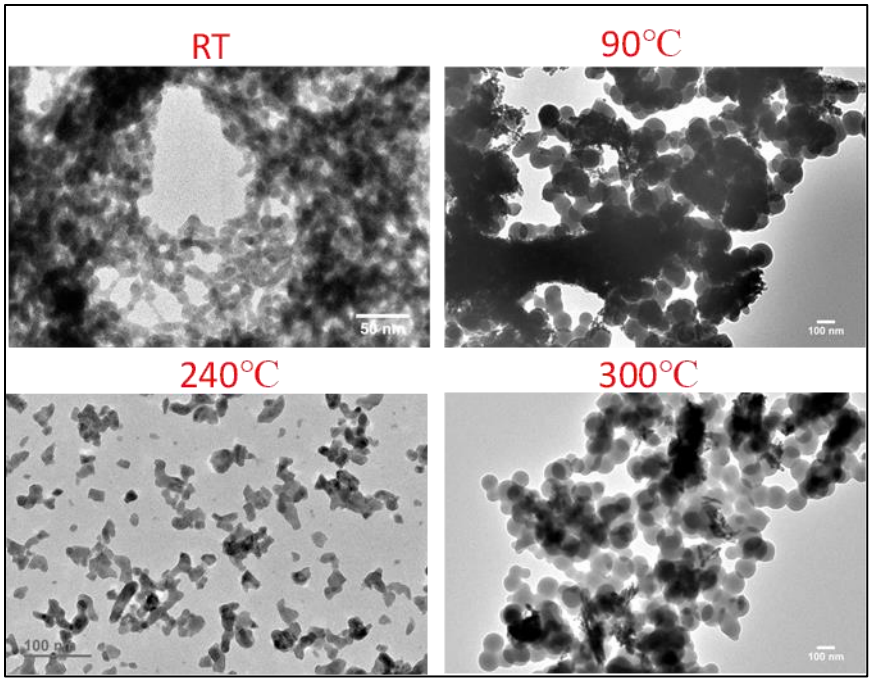

Figure 19.. TEM images of amino acid tyrosine mediated synthesized ytterbium and erbium co-doped sodium yttrium fluoride NPs at room temperature, 90, and annealed at 240 and 300°C, respectively.

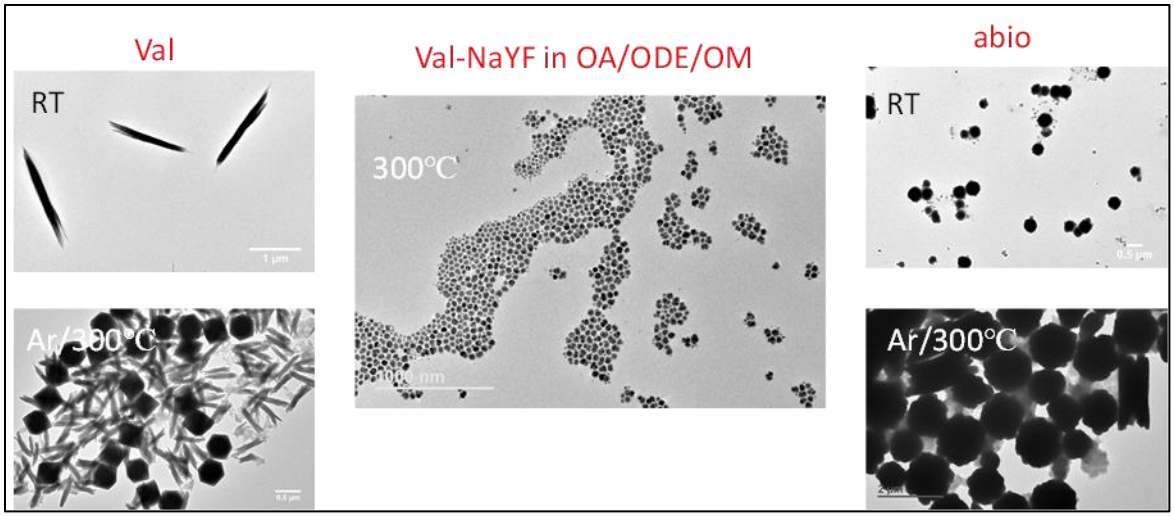

Figure 20. TEM images of valine and abiotic synthesized sodium yttrium fluoride NPs at room temperature in aqueous solutions and annealed at 300°C in Ar and in OA/ODE/OM mixed solution (central).

The room temperature as-synthesized ytterbium and erbium doped sodium yttrium fluoride sample, produced either through bio or abio-approaches, exhibited very weak up-conversion and down-conversion emissions (Figure 21a). The optically active transition of bio-REE NPs are $^{2}H_{11/2} \rightarrow {}^{4}I_{15/2}$ (523nm), $^{4}I_{13/2} \rightarrow {}^{4}I_{15/2}$ (1525nm) and the not attributed ones were at 1125 and 1350 nm. On the other hand, abio-REE NPs show weak transitions of $^{4}I_{9/2} \rightarrow {}^{4}I_{15/2}$ (808nm), 1125, 1278, 1350nm and $^{4}I_{13/2} \rightarrow {}^{4}I_{15/2}$ (1525nm). After the annealing treatment in Ar gas (Figure 21 b, c), these particles demonstrated strong up-conversion emission and down-conversion emission

peaks from the transitions of $^2H_{11/2} \rightarrow {}^4I_{15/2}$ (523nm), $^4F_{9/2} \rightarrow {}^4I_{15/2}$ (660nm) and $^4I_{13/2} \rightarrow {}^4I_{15/2}$ (1525nm).

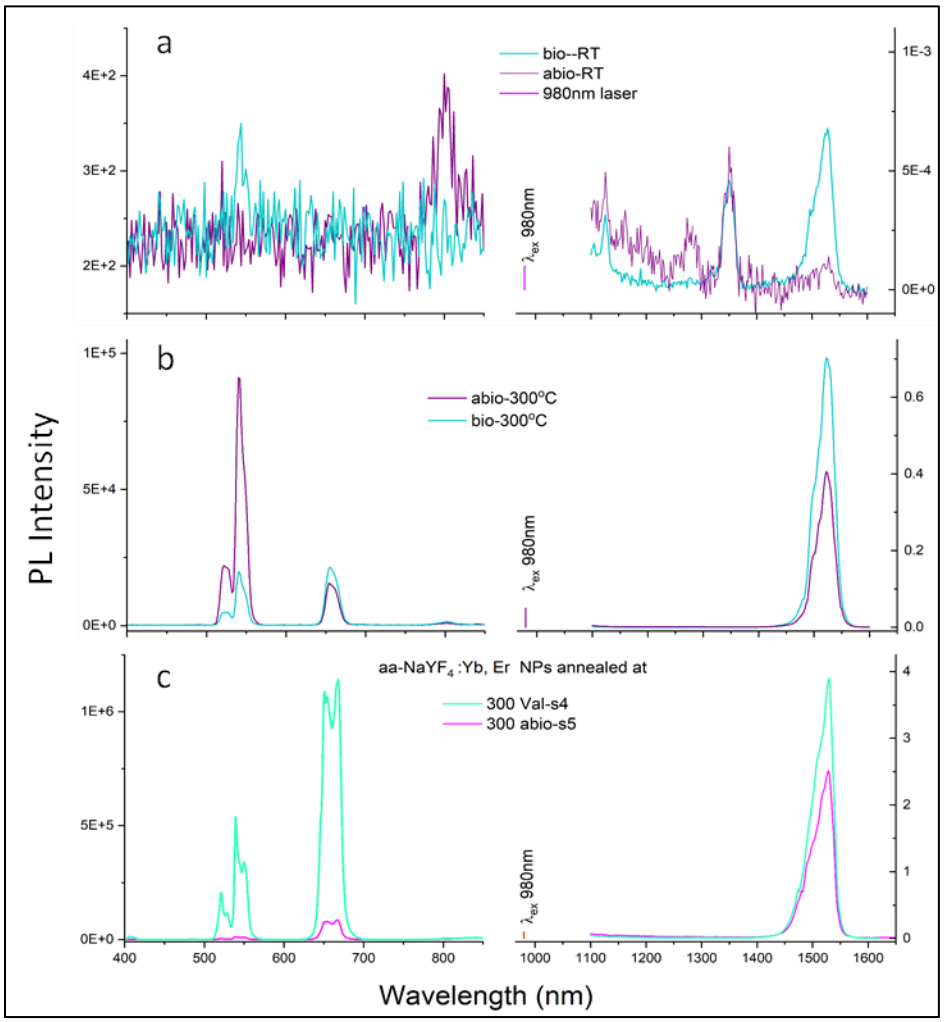

Figure 21. Comparisons of PL spectra of direct synthesized of Yb, Er doped sodium yttrium fluoride NPs. (a) and (b), with (bio) and without (abio) M13 phage mediated sodium yttrium fluoride and their annealed at 300℃ ones. (c) Amino acid valine mediated direct synthesized of Yb, Er doped sodium yttrium fluoride NPs, which have been annealed at 300℃.

We further studied core-shell nanostructures based on the room temperature amino acid (aa) mediated sodium yttrium fluoride nanoparticles as the precursor. The precursor of aa-NaYF was firstly annealed in OA/ODE/OM mixed solution to form small sized uniform particles, and then the precursors for shells of sodium and REE trifluoroacetate salts were added and heated at 300℃ to grow shell layer over the core particles. Figure 22 shows an example of glu-NaYF particles synthesized at room temperature with the core NP particles and core-shell NPs synthesized at 300℃.

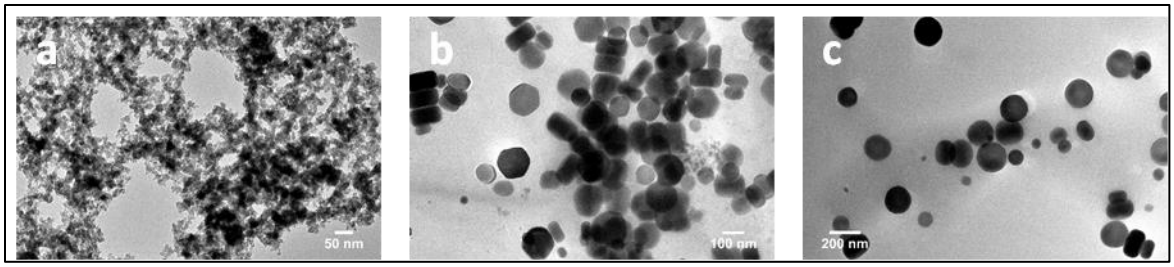

Figure 22. (a) Glu-Na1.56 Y2.44 F9.38 NPs synthesized at room temperature; (b) glu-NaYF4:Yb, Er and (c) glu-NaYF4:Yb, Er @ NaYF4 core-shell NPs synthesized at 300°C

4.2 Physical Properties of Rare-Earth Doped Oxides

Figure 2 shows the bio-MO:REE NPs synthesized with M13-phage (E3:EEAE clone) biotemplates at mild temperatures (from 21°C to 70°C). Due to limitations in the quantity of each sample and laboratory time, these samples were not treated at high temperature. The nanoparticles synthesized at lower temperatures were highly amorphous in structure, and no PL emission from the doped REE elements in the NPs could be observed. Figure 23 shows the PL spectra from bio-$SrAl_2O_4$:Eu,Dy, and images of a sample. The spectra were recorded 5 seconds after stopping the excitation light illumination.

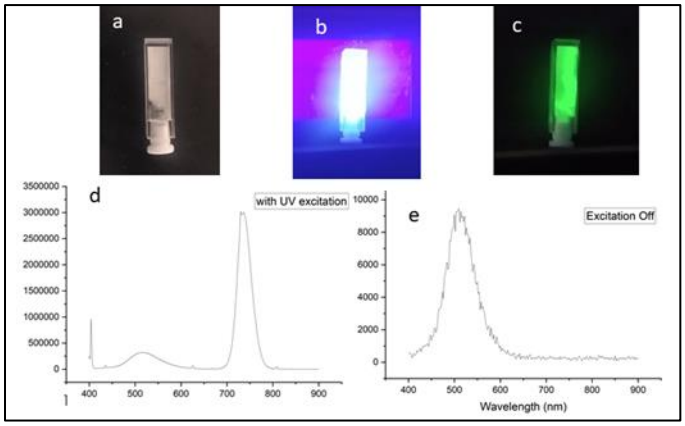

Figure 23. Bio-SrAl2O4:Dy,Eu nanoparticles treated at 950°C demonstrated 520 nm green light emission for an extended lifetime (~minutes). (a) Photo taken under normal room light, (b, d) photo and PL spectrum under UV light, and (c, e) photo and PL spectrum taken 5 s after UV illumination turned off.

4.3 Physical Properties of Rare-Earth Perovskites

Figure 24 shows TEM images of M13 phage (E3 clone) biotemplate-synthesized bio-$CsPb(OH)_x$ using an aqueous process [Figure 4(a)], which was used as the precursor for synthesis of lead halide perovskite ($CsPbX_3$:REE) NPs (X = Br, Cl; REE = Yb, Pr). TEM images of perovskite bio-$CsPbBr_3$:Yb NPs and bio-$CsPbCl_3$:Pr NPs which were synthesized at 240°C for 1 min were shown in Figure 24(b) and (c). The abiotic control $CsPbBr_3$:REE NPs were synthesized at 240°C for 1 min, and is shown in Figure 24(d). Again, chain-like phage-templated bio-$CsPb(OH)_x$ precursor nanomaterials have been obtained. Additionally, the resultant lead halide perovskite

bio-$CsPbX_3$:REE NPs also showed chain-like assembly of NPs, which is very similar to the morphology of bio-$Na(REE)F_4$ NPs in section 3.1. However, the shapes of these NPs were not as regular as the control abiotic counterpart NPs, which exhibited perfect square plate-like shapes with uniform sizes. This result is perhaps because of the local environment around seeds of bio-$CsPb(OH)_x$ due to the complex phage template surfaces, which are quite different from abiotic synthesis. Additionally, the PL spectra from bio-$CsPbCl_3$:Pr NPs and bio-$CsPbBr_3$:Yb NPs are shown in Figure 24(e). Notably, these PL emission peak intensities are very strong even under low levels of excitation light, indicating very high quantum yields for these biotemplated REE-doped lead halide perovskite nanoparticles, despite the relative lack of shape uniformity.

Interestingly, the typical f-f transition lines from REE^{3+} ions were not observed for these two sample nanomaterials. One possible explanation is that the doped REE^{3+} ions are introducing an additional impurity energy state that is located below the transition band level, and that enhances the near band-to-band optical transitions, instead of promoting direct 4f-4f electronic transitions. To confirm this hypothesis, we investigated another system REE-doped lead halide perovskite, bio-$NaSrF_3$:Tb,Eu NPs, which is a wide bandgap material; however, the doped Eu and Tb REE energy levels are close, and they could enhance the PL efficiency through energy transfer processes. The results are shown in Figure 25.

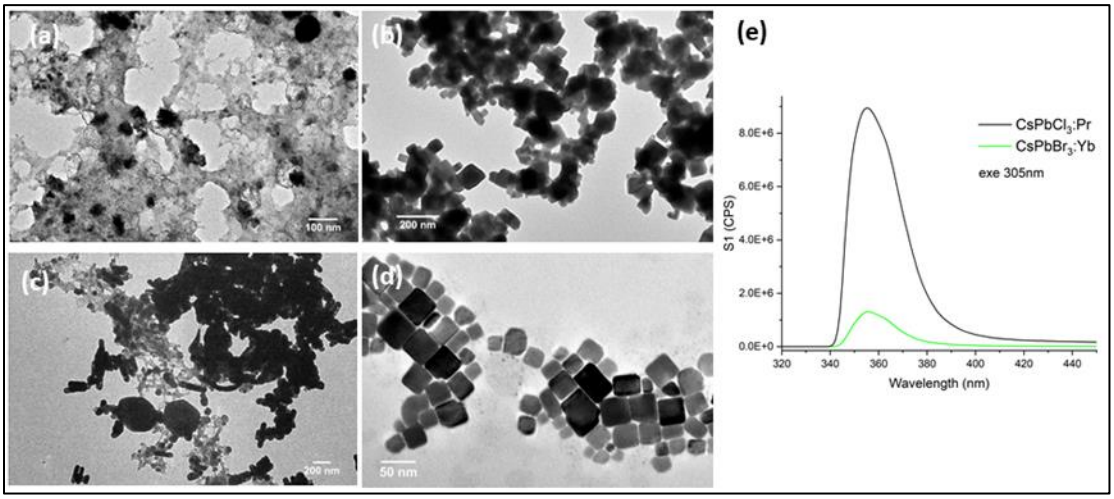

Figure 24. (a) M13 phage (E3 clone) biotemplated bio CsPb(OH)x synthesized using an aqueous process. (b) Perovskite bio-CsPbBr3:Yb NPs synthesized at 240°C for 1 min. (c) Perovskite bio-CsPbCl3:Pr NPs synthesized at 240°C for 1 min. (d) Abiotic CsPbBr3:REE NPs synthesized at 240°C for 1 min. (e) PL spectra from bio-CsPbCl3: Pr NPs and CsPbBr3:Yb NPs.

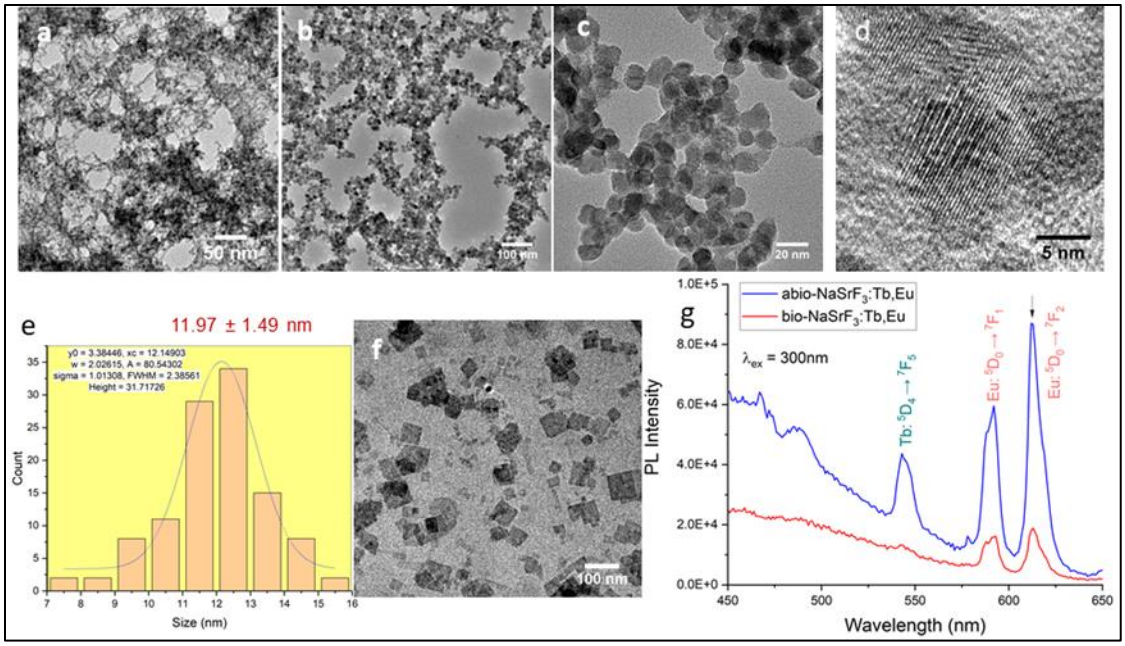

Figure 25. Synthesis of bio-NaSrF3:Tb,Eu NPs with M13 bacteriophage biotemplates and the abiotic control nanoparticles under the same conditions. (a) bio-SrTbEu-(OH)x precursor synthesized using an aqueous process. (b-d) TEM images of Bio-NaSrF3:Tb,Eu NPs synthesized in organic solvent and viewed at different magnifications. (e) The NP size distribution of bio-NaSrF3:Tb,Eu particles. (f) TEM image of abiotic (abio) NaSrF3:Tb,Eu NPs. (g) The region of PL spectra of bio-NaSrF3:Tb,Eu NPs and abiotic (abio) NaSrF3:Tb,Eu NPs having narrow emission peaks arising from the 4f-4f optical transitions of REE3+ ions.

We synthesized and studied Tb^{3+} and Eu^{3+} co-doped $NaSrF_3$ NPs through bio- and abio-approaches. Unlike the case in REE in $CsPbX_3$, that no f-f optical transition could be observed, several narrow emission bands were observed. These are the very typical 4f-4f optical transition from Eu^{3+} and Tb^{3+} ions. The red emission bands are corresponding to the transition $^5D_0$–^7F_J (J = 1–6) of Eu^{3+} (593nm and 613nm peaks originate from the $^5D_4 \rightarrow {}^7F_1$, $^5D_4 \rightarrow {}^7F_2$). And the green emission (544nm) is attributed to the transition of $^5D_4$–$^7F_5$ of Tb^{3+}. The fact suggests that the difference of interaction between Pb^{2+} and Sr^{2+} with the REE^{3+} in the hosting materials.

4.4 Rare-Earth Organic-Inorganic Core-Shell NPs

In our research, we have focused on the bio-$Na(REE)F_4$ systems in section 3.1 and the core-shell NPs discussed in sections 3.2 and 3.3. The biologically synthesized rare-earth organic-inorganic core-shell NPs that were already designed, produced, and analyzed in the previous sections are listed in Tables 2 and 3, and as follows: $NaYF_4$:Yb,Er@$NaYF_4$:Yb; $NaYF_4$:Yb,Tm@$NaYF_4$:Yb; $NaYbF_4$:Er,Ce,Zn@$NaYF_4$:Yb; and $NaYF_4$:Yb,Er@$NaYF_4$:Yb,Er@$NaYF_4$:Yb. There is no additional data to report for this section.

4.4.1 Tables of All Synthesized Materials Produced (Abiotic and Biotic)

Table 2. Nanoparticles produced via biogenic synthesis methods

		Sodium Rare-Earth Fluorides	Rare-Earth Doped Oxides	Rare-Earth Perovskites	Rare-Earth Organic-Inorganic Core-Shell NPs
		$NaYF_4$:Yb,Er	SrO:Eu	$CsPbCl_3$:Pr	$NaYF_4$:Yb,Er@$NaYF_4$:Yb
		$NaYF_4$:Yb,Tm	SrO:Pr	$CsPbBr_3$:Yb	$NaYF_4$:Yb,Tm@$NaYF_4$:Yb
		$NaYbF_4$:Er,Ce,Zn	YO:Eu	$NaSrF_3$:Eu,Tb	$NaYbF_4$:Er, Ce, Zn@$NaYF_4$:Yb
		$NaYF_4$:Yb,Er, Tm	ZnO:Eu		$NaYF_4$:Yb,Er@$NaYF_4$:Yb,Er@$NaYF_4$:Yb
			$SrAl_2O_4$:Eu^{2+}, Dy^{3+}		
			$SrAl_2O_4$:Eu^{2+}, Nd^{3+}		

Table 3. Nanoparticles produced via abiotic synthesis methods

	Sodium Rare-Earth Fluorides	Rare-Earth Doped Oxides	Rare-Earth Perovskites	Rare-Earth Organic-Inorganic Core-Shell NPs
	$NaYF_4$:Yb,Er	SrO:Eu	$CsPbCl_3$:Pr	$NaYF_4$:Yb,Er@$NaYF_4$:Yb
	$NaYF_4$:Yb,Tm	ZnO:Eu	$CsPbBr_3$:Yb	$NaYF_4$:Yb,Tm@$NaYF_4$:Yb
	$NaYbF_4$:Er,Ce,Zn	$SrAl_2O_4$: Eu^{2+},Dy^{3+}	$CsPbCl_{3-x}Br_x$:Eu	$NaYbF_4$:Er, Ce, Zn@$NaYF_4$:Yb
	$NaYF_4$:Yb,Tm,Nd		$NaSrF_3$:Eu,Tb	$NaYF_4$:Yb,Er@$NaYF_4$:Yb,Er@$NaYF_4$:Yb
	$NaYbF_4$:Er		$LaYO_x$:Nd	
	$NaYF_4$:Er Tm		$LaInO_x$:Eu	
	$NaYF_4$:Yb,Er,Tm		$YAlO_x$:Ce,Eu	

Table 4. Aqueous solution amino acid mediated synthesized sodium yttrium fluoride NPs

Amino Acid	aa-REE Yield, mg*	Shape	Lattice Structure**	Final pH
Histidine	183.34	wire	hex	
Lysine	206.11	wire	am	
Methionine	142.22		cubic	
Phenylalanine	213.27	wire	hex	
Glutamine	187.59		cubic	4.31, 5.08
Glycine	124.66	belt	cubic	4.65
Leucine	177			5.79
Alanine	160		hex	5.46, 5.64
Arginine	140	wire	am	9.57, 9.68
Asparagine	208.18	wire	hex	
Threonine	206.5	wire	am	
Tryptophan	224.25	wire	am	1.82
Isoleucine	133.4	belt	hex	2.11
Tyrosine	174.09	wire	am	
Cysteine	126.91	sphere	am	1.46, 2.33
Proline	201.66	wire	am	
Serine	243.11	wire	am	
Valine	215.35	belt		5.9

*** 1 mmol sodium yttrium fluoride scale synthesis**
**** hex: hexagonal, am: amorphous**

4.5 Study on Phage Binding Rare Earth Ions

Understanding the interactions between phage proteins and REE ions in solution, or the ability of phage to bind to REE ions (affinity) is the basis of this section. Since different sequenced phages could possess different binding abilities for different REE ions, resulting in variations in the final as-synthesized bio-REE NP products, such as the non-uniform stoichiometry, shape, size and nanostructure, and thus imparting different physical properties and functionality. We have investigated the interactions of EEAE (E3), CPDC (Cys), DSPH, GTGTCG (P8#9) and AEGB (wild-type) M13 phage clones with all 15 rare-earth element ions (including Y, but excluding Pm). The experiments were carried out at low pH values in mixed REE ion solutions with equal concentrations of each REE ion in a solution phase. Above pH 4, a fraction of the REE ions will exist in REE-hydroxide complexes, and precipitate from solution, so all the experiments were conducted at pH below 3.0. For the pH = 0 case, we combined M13 phage in suspension with REE^{3+} ions (1.5% nitric acid, 40 ppm REE^{3+} ions, 7.5E11/mL phage), then mixed at 200 rpm for 4 hours with a bio-shaker, and then filtered the phage-REE particles through 0.2-µm filters. We measured the REE^{3+} concentration of the filtrate using an inductively coupled plasma - optical emission spectrometer (ICP-OES) to determine the concentration of REE ions that bound to the phages.

Figure 26 shows after interaction of phage with REE ions, the REE concentration changes from the initial REE concentrations at different pH values. It is seen that for case of pH = 0, the phage have the lowest REE binding ability, but still there were 2.5% to 9% reduction in REE concentration due to the binding of phage, and wild-type phage had the smallest binding affinity, whereas the CYS phage clone had the strongest binding ability. Thus, the data plots demonstrate that, in acidic solutions at a given pH value, different phage clones show different abilities to bind to different REE ions. At pH 1.5 and 2.9, the phage clones displayed similar trends for different REE ions, for example, Y, Pr, and Lu ions were much weaker than other REE ions bonded to the phages. Figure 27 plots the ability of each phage clone to bind to different REE ions at different pH values in solution. Again, we see that for each phage clone, the binding affinity for different ions varies. This is helpful information when we synthesize bio-REE NPs containing multiple REE ions, because these differences could result in differences in stoichiometry of the final products. Furthermore, these data will also provide useful information for bio-mining (bio-leaching) and bio-extraction of REEs in the mining industry.

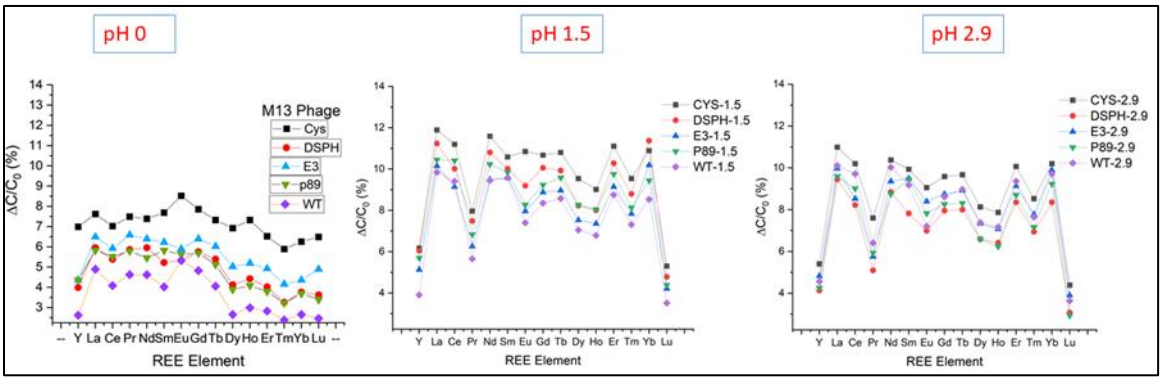

Figure 26. Changes in REE ion concentrations in REE solutions at different pH values after interaction with different M13 phage clones.

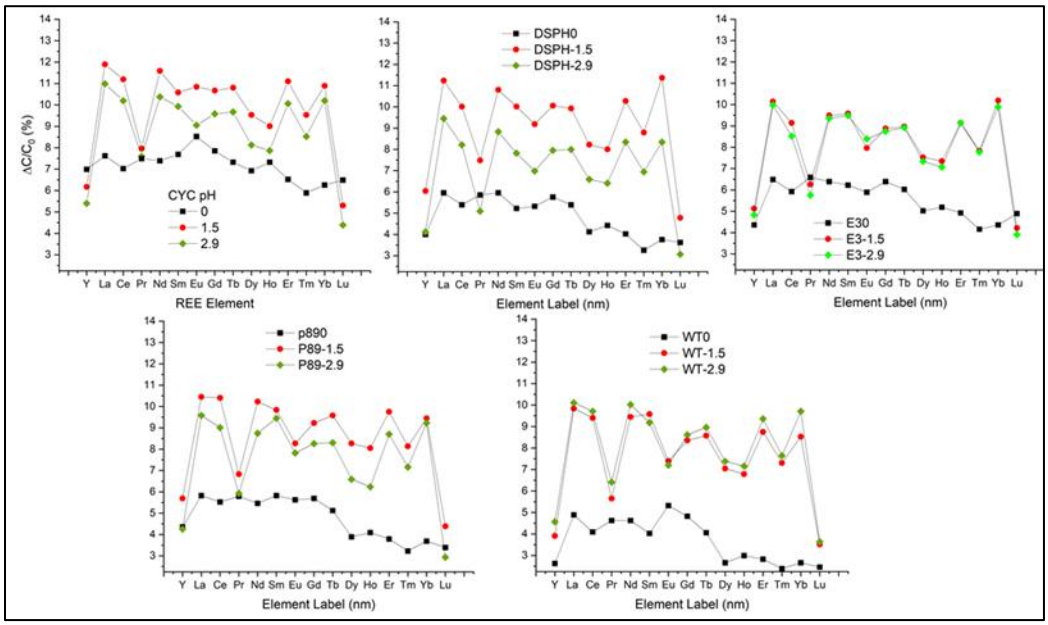

Figure 27. Ability of M13 bacteriophage CYC, DSPH, EEAE, p89 and wild-type clones to bind to different REE3+ ions in acidic solutions (pH: 0, 1.5, and 2.9).

5.0 CONCLUSIONS

5.1 Effort Highlights

To the best of our knowledge, there has been no previously successful synthesis of sodium rare-earth fluoride NPs under mild aqueous conditions, nor using a biosynthesis approach, and all previous synthesis methods have required high temperatures and organic solvents. The same situation is present for synthesis of lead halide perovskite NPs, and no successful aqueous synthesis of bio-lead halide perovskites have been reported to the best of our knowledge.

Our first effort in this project is to develop an effective experimental approach to overcome the difficulties in biological assisted synthesis of bio-sodium rare-earth fluoride NPs and bio-lead halide perovskite NPs. We developed the aqueous solution synthesis of bio-REE-OH NPs as the precursors to synthesize sodium rare-earth fluoride NPs as well as halide perovskite (bio-$CsPbX_3$:REE) NPs in organic solvents. Furthermore, this aqueous solution synthesis also works for REE-doped bio-oxide NPs (or bio-perovskite oxide NPs).

In short, the aqueous solution synthesis of bio-REE-OH is the key step in the project research, which enables us to obtain:

1) Aqueous solution synthesis with the assistance of biological systems (e.g., M13 phage biotemplates).

2) Precursors for successful synthesis of sodium rare-earth fluoride NPs in organic solvents.

3) Precursors for successful synthesis of lead halide perovskite NPs in organic solvents.

4) Precursors for synthesis of REE-doped oxide NPs at high temperature.

In addition, we have made effort on following topics to meet the milestones of the project: particle size control, uniformity control, PL efficiency, PL emission Stokes shift (anti-Stokes shift), core-shell structures, and control of material stoichiometry.

5.2 Accomplishments

We fulfilled the following proposed milestones for this project:

Month 2: Demonstrate the ability to use a bioengineering approach to change the identity of specific REE incorporated within the structure of a biosynthesized inorganic nanoparticle for ≥ 2 different REEs.

Month 3: Engineer a biological system to produce, and then test, functional REE-containing nanoparticles: Demonstrate a single biogenic nanoparticle composition that absorbs and emits light in the visible (400 – 700 nm) or near-IR (NIR, 700 nm – 1500 nm) with an up-converting or down-converting mechanism.

Month 4: Demonstrate ability to engineer a biological system to produce similarly sized nanoparticles (width of all particles < 50 nm).

Month 6: Expand the bioengineering capabilities to enable more complex REE-containing nanoparticle structures by fabricating a nanoparticle surface layer (intended to enhance its performance or stability, e.g., a shell) with consistent composition and thickness (< 20% standard deviation).

Month 6: Extend ability to use engineered biological systems to tune the functional performance of REE-containing nanoparticles: Demonstrate 5 distinct nanoparticle compositions that up-convert and/or down-convert visible and/or NIR light with a Stokes shift > 50 nm.

Month 9: Demonstrate the use of engineered biological systems to interchangeably incorporate ≥ 3 different REEs into a functional nanoparticle, to illustrate the following: Incorporation of different REEs into up-converting/down-converting nanoparticles influences Vis/NIR absorption/emission properties. At least 1 resultant biogenic REE nanoparticle formulation should yield > 100 nm Stokes shift and > 15% QE.

Month 11: Utilize engineered biological systems to adjust the stoichiometric ratio of REEs incorporated into nanoparticles, to demonstrate that: bio-driven control of REEs stoichiometry in nanoparticles results in changes in Vis/NIR optical properties (as noted above) (80% complete).

Month 12: Demonstrate an engineered biological system that produces REE-containing nanoparticles of a defined size range: Demonstrate control of the size of REE-containing, core-shell nanoparticles that results in changes in Vis/NIR optical properties (as noted above). Size should range from 5 nm to 30 nm with a distribution range of < 10 nm. (100% complete).

Month 12: Provide a status report detailing and comparing attributes and limitations of their biogenic materials to conventionally prepared materials, including their synthesis, composition, and performance.

Month 15: Develop an engineered biological system that enables tuning of multiple features of synthesized nanoparticles (e.g., REE content, composition, size, architecture), which demonstrate the following functional performance metrics: Deliver ≥ 2 distinct REE-containing biogenic particle formulations that absorb and emit in either the Visible or NIR ranges, with single-peak wavelength emission with a < 50 nm FWHM; > 25% QEs; > 200 nm Stokes shift between absorption and emission.

5.3 Technical Challenges

To the best of our knowledge, there has been no previous successful synthesis of sodium rare-earth fluoride NPs under mild aqueous conditions, as well as using the bio-synthesis approach, and all previous synthesis methods require high temperatures and organic solvents. The same situation is for synthesis of lead halide perovskite NPs, and no successful aqueous synthesis of bio-lead halide perovskite has been reported to the best of our knowledge. Our innovative solutions required our

deep nanomaterials synthesis expertise and exceptional creativity in order to develop two first-in-class nanoparticle compositions under mild, aqueous conditions.

The technical challenges that we encountered were:

1) Sodium rare-earth fluoride NPs and lead halide perovskite NPs could not be synthesized in biologically compatible aqueous solutions due to auto-oxidation.

2) Most biological systems or templates cannot persist in organic solvents over a relatively long period of reaction time, especially when the temperature is above 200°C.

3) For the biologically assisted synthesis of bio-REE NPs, the approach to control the particle size, uniformity of size and shape, PL efficiency, and material stoichiometry among the multiple elements in the NPs.

A non-technical challenge that we encountered is that the research project timeline was too short for so many tasks and milestones, especially since each bio-synthesis method required a long period of time to complete a single trial (or cycle) of an experiment.

5.4 Future Directions

The synthesis approaches developed in the project could provide alternate methods to produce very small, uniform high-emission, high-quantum yield biotemplated REE NPs (size <15 nm, QE >30%), and 1D and 2D nanomaterials under mild, aqueous conditions, which could be useful in many important applications such as biomedical near-infrared (NIR) imaging probes, photovoltaic devices, and phosphors for LEDs. The study of phage protein-REE ion interactions under aqueous conditions could also provide us with helpful information for higher yield bio-mining and biosynthesis of REEs in solution phases.

6.0 REFERENCES

1. Optical Spectra and Energy Levels of Erbium-Doped Yttrium Orthoaluminate, Vincent L. Donlan; Abraham A. Santiago, Jr. *J. Chem. Phys.*57, 4717–4723 (1972).

2. Indumathi Kamma, Monday Mbila, Karen E. Steege Gall, and B. Rami Reddy, Optical Materials Express 3 (6), pp. 884-892 (2013).

3. S Heer, K Kompe, HU Gudel, M Haase, Highly efficient multicolour upconversion emission in transparent colloids of lanthanide-doped NaYF4 nanocrystals, Advanced Materials, 2004.

4. Meng Ju, MingMin Zhong, Cheng Lu, and Yau-yuen Yeung, Deciphering the Microstructure and Energy-Level Splitting of Tm^{3+}-Doped Yttrium Aluminum Garnet, Inorg. Chem. 2019, 58, 1058−1066.

5. C Tiseanu, A Lupei, and V Lupei, Energy levels of Tm^{3+} in yttrium aluminium garnet J. Phys.: Condens. Matter 1995, 7, 8477-8486.

6. Simone Normani, Pavel Loiko, Liza Basyrova, Abdelmjid Benayad, Alain Braud, Elena Dunina, Liudmila Fomicheva, Alexey Kornienko, Ammar Hideur, and Patrice Camy, **Optical Materials Express,** Vol. 13, Issue 7, pp. 1836-1851, (2023). https://doi.org/10.1364/OME.482402.

7. H. Isshiki et al. Fine structure in the Er-related emission spectrum, Journal of Luminescence 102–103 (2003) 819–824.

LIST OF SYMBOLS, ABBREVIATIONS, AND ACRONYMS

AFRL	Air Force Research Laboratory
Cys	CPDC M13 phage
E3	EEAE M13 phage
ICP-OES	Inductively Coupled Plasma - Optical Emission Spectrometer
NIR	Near-IR (700 nm – 1500 nm
NPs	Nanoparticles
OA	Oleic Acid
ODE	1-Octadecene
OM	Oleylamine
QY	Quantum Yield
REEs	Rare Earth Elements
RX	Materials and Manufacturing Directorate
RXE	Photonics, Electronics, and Soft Materials Division
RXEB	Biomaterials Branch
USAF	United States Air Forse
WPAFB	Wright-Patterson Air Force Base